Natural remobilization and historical evolution of a modern coastal transgressive dunefield

Nicolas Robin, Julie Billy, Alexandre Nicolae Lerma, Bruno Castelle, Patrick A Hesp, David Rosebery, Corentin Fauny, Jacques Deparis, Vincent Marieu, Cedric Bouchet, et al.

Robin Nicolas (Orcid ID: 0000-0003-2323-2552)
Billy Julie (Orcid ID: 0000-0002-8817-355X)
Hesp Patrick Alan (Orcid ID: 0000-0003-4573-2945)

1 Natural remobilization and historical evolution of a modern coastal transgressive dunefield

Robin N [1], Billy J [2], Nicolae Lerma A [3], Castelle B [4], Hesp P.A. [5], Rosebery D [6], Fauny C [1, 3], Deparis J [6], Marieu V [3], Bouchet C [6], Miot da Silva, G.[5].

[1] CEFREM, UMR CNRS 5110, Université de Perpignan Via-Domitia, Perpignan, France.

[2] BRGM French Geological Survey, Risks and Prevention Division, Orléans, France.

[3] BRGM French Geological Survey, Regional Direction Nouvelle-Aquitaine, Pessac, France.

[4] CNRS, Université de Bordeaux, UMR 5805 EPOC, Pessac, France.

[5] Beach and Dune Systems (BEADS) Laboratory, College of Science & Engineering, Flinders University, Adelaide, Australia.

[6] Office National des Forêts, Paris, France.

Corresponding author: Nicolas.robin@univ-perp.fr

This article has been accepted for publication and undergone full peer review but has not been through the copyediting, typesetting, pagination and proofreading process which may lead to differences between this version and the Version of Record. Please cite this article as doi: 10.1002/esp.5535

Abstract

The vast majority of coastal dunes in Europe have been stabilized by increasing vegetation cover since the mid-20th Century. However, some systems may experience a remobilization phase, generally occurring locally and further propagating alongshore, the drivers of which remain poorly documented. This study investigates the evolutionary paths (stabilization/destabilization/remobilization) from 1945 to 2020 of a 2-km long modern coastal transgressive dunefield located in southwest France with a holistic approach (GPR profiles, aerial photographs and LiDAR topographic data). Results show a landward migration of the transgressive dune by approximately 233 m +/- 7.5m, through two distinct stages of rapid landward migration from 10 to 23 m/year (Stage I: 1949-1959 and Stage III: 2000-2021) separated by an approximately 40-year stage of slow to no migration, but with substantial windward slope deflation (Stage II). The onset of stage II is due to the fixation of vegetation by human action between 1950 and 1959. The onset of stage III is hypothesized to be driven by long and sustained upper backshore/dune toe erosion beginning in 1968 due to a massive shoal welding that locally disturbed the longshore drift. It induced a destabilization of the dune and erosion of the vegetation cover over some decades. A non-synchronization is therefore observed between the start of the perturbation (1968), then the migration (2000) in line with the hysteresis concept of Tsoar (2005). This study shows that almost all of the sedimentary volume of the 1945's dune has been remobilized by translation to shape the dune system in its current form. The 2.2-km dunefield has grown by approximately 673,000 m^3 +/- 190,000 m^3 during the 2005-2020 period. Among this volume, there is a new foredune that was built from 2005 between the upper beach and the transgressive dune (volume in 2020 of about 394,000 m^3 +/- 68,000 m^3).

Keys words (5): Dunefield evolution; Foredune; GPR; sandwave, shoal welding

2 Introduction

Transgressive coastal dunefields are common on many coasts of the world. They particularly dominate coastlines characterized by higher wave and wind energy environments, and/or arid environments with moderate to high sediment supply but also in humid and tropical environments where there is a defined dry season (cf. reviews of Hesp, 2011, 2013a). The term transgressive dunefield was first coined by Gardner (1955) to describe relatively large scale, mobile (active) coastal dunefields on the east coast of Australia. The term 'transgressive' was used because the dunefields typically 'transgress' (migrate over) prior terrain. Hesp and Thom (1990) subsequently noted that the term can refer to both mobile (or active), semi-stabilized (active and vegetated parts) or stabilized (vegetated) systems. They occur as normal, oblique and alongshore migrating dunefields (Hesp, 2013a). The surface of active transgressive dunefields are commonly covered with a large variety of landform units including parabolic and barchans dunes, transverse/oblique dunes, deflation plains and basins, nebkha, remnant knobs and blowouts (cf. reviews of Hesp, 2011, 2013a). They are similar to ergs or sand seas of continental dunfields.

Many transgressive dunefields in temperate environments have experienced sedimentary mobility that persisted until the beginning of the 20th century (Tsoar and Blumberg, 2002; Martinho et al., 2010; Miot da Silva and Hesp 2013; Mendes and Giannini, 2015; Pickart and Hesp, 2019; Rocket et al., 2021). Since then, there has been a tendency toward stabilization and vegetation colonization, particularly in the northern hemisphere (Provoost et al., 2011; Jackson et al., 2019a; Moulton et al., 2019; Gao et al., 2020, 2021). Several factors have frequently been inferred as possible causes for the "greening", including anthropogenic pressure, industrial agents (e.g. nitrogen), semi-natural factors, and climatic-derived changes (Provoost et al., 2011; Gonzalez-Villanueva et al., 2013, Jackson et al., 2019a). The shift from stabilized and predominantly vegetated state to active and largely unvegetated state is identified at the small sand drift or blowout scale, but studies at larger spatial scales involving transgressive dunefields are less common. The evolutionary paths towards this state may vary considerably due to the complex morphology of these landforms. Several key factors concerning the remobilization of modern transgressive dunefields have been identified such as climate variability (Gonzalez-Villanueva et al., 2013; Mendes and Giannini, 2015), coalescence of parabolic dunes (Hesp and Thom, 1990), development of blowouts (Barchyn and Hugenholtz, 2013), fires (Filion, 1984), or water table changes (Seeliger, 2003) (see extensive review in Hesp et al., 2022). A severe storm inducing a destruction of a dune system

by large scale erosion and overwash, and the development of a transgressive dunefield has been documented in a single case (Mathew et al., 2010). It is suggested by multiple authors that sustained foredune erosion can also be a driver (Short and Hesp, 1982; Pye, 1990; Hesp and Thom, 1990; Jackson et al., 2019b). However, Hesp et al., (2022) note that there is little actual proof or evidence of this, and quite possibly none. Only Hesp et al., (2022) showed that prolonged or constant shoreline erosion and subsequent cannibalization of a relict vegetated dunefield resulted in the formation of a transgressive dunefield in South Australia.

The sediment supply from nearshore to the beach can become a source for aeolian sand transport to a foredune or dunefield (Short, 1988; Aagaard et al., 2004; Miot da Silva and Hesp, 2019). It can be manifested by onshore intertidal bar migration or nearshore bar (or shoals and swash bars) migration and welding to the beach. Their impacts depend on the synchronization of sediment supply and transport events (Houser, 2009), and if shoals are capable of substantially and persistently increasing the beach width (Galiforni-Silva et al., 2020). However, the welding bar can also disturb the littoral drift and drive foredune erosion on the downdrift end (Davidson-Arnott and Van Heyningen, 2003; Robin and Levoy 2007; Robin et al., 2009, 2020a). This latter case is not documented in transgressive dune evolution. Lastly, anthropogenic influences are also more and more responsible factors influencing dune remobilization (Arens et al., 2004; Delgado-Fernandez et al., 2019; Portz et al., 2021). Although these factors are varied and abundant, many authors argue that the actual mechanisms responsible for the reactivation of aeolian activity in coastal systems remains poorly understood (Barchyn and Hugenholtz, 2013; Gonzalez-Villanueva et al., 2013; Hesp, 2013a; Jackson et al., 2019b; Gao et al., 2020; Hesp et al., 2022). Given that vegetation is the main stabilizing agent, investigating the mechanism(s) that trigger changes in vegetation cover and the time scales involved is important.

Studies on modern transgressive dunes are relatively limited in terms of their evolution in relation to changing vegetation cover since the mid-20th Century (Tsoar & Blumberg, 2002, Marcomini and Maidana, 2006; Miot da Silva & Hesp, 2013, Mendes and Giannini, 2015, Pickard and Hesp, 2019, Moulton et al., 2019, 2020). These studies utilized aerial photography mapping to determine planview dunefield change which is a relevant method but can be limited when examining the morphological evolution taking place within the system. In contrast to literature on foredunes, current knowledge about quantification of transported/mobilized volumes, sedimentary budget and detailed topographic changes affecting a transgressive dune system are still scarce. For example, it can be difficult to link surfzone-beach sediment supply to dune building and migration and thus, if dune movement takes place at a constant volumetric

input or not. Only a few studies have documented the topographic evolution of transgressive dunefields, with transects (*e.g.* Munoz-Perez et al., 2009; Mathew et al., 2010; Davidson et al., 2021; Hesp et al., 2022) or digital elevation models (DEMs) (*e.g.* Gonzalez-Martin et al., 2021 (2 surveys); Perez-Alberti et al., 2021 (3 surveys)). Morphological and evolutionary changes in dunes are also recorded by the internal sedimentary structures. Several studies based on ground penetrating radar survey (GPR) make it possible to roughly examine the mechanisms of migration and the associated topographic evolution of transgressive dunefields during the Mid to Late Holocene period (Botha et al., 2003; Pedersen and Clemmensen, 2005; Clemmensen et al., 2007) or recent period (Buynevich et al., 2007, 2010; Costas et al., 2006; Girardi and Davis, 2010; Costas et al., 2012; Lindhorst and Betzler, 2016; Silveira et al., 2022). However, they suffer from a small-scale mapping and/or from a low chrono-stratigraphic framework resolution. So, given the potential socio-economic and environmental implications of transgressive dune mobility, a better understanding of the sediment budget is desirable and can produce useful information to future coastal management.

The aim of this study is to investigate the evolutionary processes of a transgressive dunefield located on the backshore near the Arcachon inlet on the Aquitaine coast (southwest France) between 1945 and 2020. The field site is in an unmanaged dunefield at least since the end of the 1950's and two periods of mobility punctuated by a long period of stability are identified. The study is based on a holistic approach, combining GPR cross-shore and longshore profiles, historical aerial photographs, and LiDAR topographic surveys. The overall study had three primary objectives:

(1) identify the factor(s) that control(s) the stabilization (e.g no landward migration and dune building), destabilization (e.g no landward migration and erosional morphological state) or remobilization (e.g landward migration) of the system and on what time scale these take place to reach a new state.

(2) attempt to estimate the amplitude of topographic changes before 2005 and to quantify the annual sediment budget of the system since 2005 and its fluctuation. One particular area of attention will be to understand how the beach-dune supply evolves during the migration phase of the transgressive dunefield and its distance from the coastline.

(3) observe the relationships between the transgressive dunefield migration and the initiation of a new foredune.

3 Field site

The Aquitaine coast beach-dune system in southwest France extends approximately 230 km from the Gironde estuary in the north to the Adour estuary in the south (Figure 1). Beaches are mostly intermediate, doubled barred types (Lafon et al., 2002; Castelle et al., 2007) and the dune system comprises one of the longest and largest dune systems in Europe (Bossard and Nicolae Lerma 2020).

The coast is a wave-dominated, meso-macro-tidal environment with an annual mean spring tidal range of 3.7 m with a maximum reaching 5 m during high spring tides (Castelle et al., 2007). The wave climate is energetic and strongly seasonally modulated with a monthly-averaged significant wave height Hs (and peak wave period Tp), ranging from 1.1 m (8.5 s) in July with a dominant west-northwest direction, to 2.4 m (13 s) in January with a dominant west direction (Castelle et al., 2017). Wave height can exceed 11 m during winter storms (Nicolae Lerma et al., 2015). The net longshore drift is mostly oriented southward along most of the coast (Idier et al., 2013), except along northwest-facing sectors where the longshore drift reverses. Winter winds mainly come from the west whereas dominant spring and summer winds come from north to north-west (Nicolae Lerma et al., 2019) (Figure 1), driving a dominant eastwards aeolian sand transport. Previous studies have reported an estimated aeolian flux on the Aquitaine coast of about 15-30 $m^3/m/yr$ (Froidefond and Prud'homme, 1991).

This work focuses on a part of the coastal dune system of the Aquitaine coast, located 5 km South of the Arcachon lagoon inlet and locally named "The Trencat" (Figures 1b, c). This 2.2-km long dunefield, located in a military zone, has been in free evolution at least since the end of 1950's. The coastal dunes are currently composed by a foredune (10 m NGF high), and an active (predominantly unvegetated) transgressive dune up to 20 m NGF high and 350 m wide, which is migrating into the inland pine forest (Figure 1c). The dunefield has a few blowouts, parabolic dunes and deflation basins in the southern section. This sector contrasts with the adjacent coastal dunes landscape which have been managed by the National Forest Office (ONF) (sand-fences, marram grass planting, reshaping…) since the 18^{th} century (Bossard and Nicolae Lerma, 2020; Robin et al., 2021). Behind the present coastline, the area is composed of discrete dune systems successively built over the Late Holocene (Tastet and Pontee, 1998). Along the Trencat dune, the residual longshore drift is southward oriented, largely influenced by Arcachon inlet hydro-morphodynamic. The evolution of this stretch of the coast is controlled by occasional shoal welding, reported to be of variable size (Michel et al., 1995; Lafon et al., 2000; Burvingt et al., 2022). This welding generating massive sand wave attached

at the coast causes large sediment supply as well as perturbation of the hydro-sedimentary process at multi-year to multi-decadal time scale. For instance, the larger on the recent history (called hereinafter the large welding) occurs in the 1950's, with the resulting large sand bulge further diffusing and migrating southwards at an estimated rate of 150 m/year between 1959 and 1993 (Michel et al., 1995), thus affecting the Trencat beach and dune system (Figure 2).

4 Methods and data

The Trencat coastal dune system was investigated using a combined approach with GPR profiles, aerial photographs and LiDAR topographic data. In order to address the alongshore variability of the freely evolving dunefield behavior, the Trencat zone was divided into six natural areas (named N_2 to N_7; Figure 1c). The adjacent northern and southern managed areas (named M_1 and M_8) were also included in the study.

4.1 Aerial photographs from 1947 to 2020

Aerial photographs from 1945 to 2020 were gathered. Twenty photographs taken by the French National Geographic Institute (IGN, data available on line: https://remonterletemps.ign.fr) (1945, 1947, 1950, 1959, 1964, 1968, 1973, 1979, 1982, 1985, 1991, 1996, 1998) and by the Observatoire de la Côte de Nouvelle-Aquitaine (OCNA) (2000, 2005, 2009, 2011, 2016, 2019, 2020) were analyzed using ArcGIS software and ArcGIS DSAS 5.0 (Oyedotun, 2014). IGN raster were georeferenced to the orthophotograph of 2020 (pixel size of 0.1 m). Once the calibration points were set, a transformation model computed the resulting mean quadratic error between the real X, Y coordinates of a point and the coordinates calculed by georeferencing. At least 30 landmarks were identified on each photograph, and root mean square errors of <3 m were considered acceptable. Ortophotographs between 2000 and 2020 were processing by OCNA with a root mean square errors of <0.2 m. The table 1 computed detailed and uncertainties of each photographs.

Salient geomorphologic limits were identified in order to analyze the coastal dune landscape and vegetation cover variability and trends. Several indicators were digitized: (i) the foredune (dune) foot L_{df} , as the permanent vegetation limit or dune toe which corresponds often to a well-defined break (or scarp during stage II) of slope separating the upper beach from the foredune, (ii) the landward limit L_{wl} between the dune (with sand) and woodland which has a dense and easily recognizable vegetation cover (often pine forest). It is considered as near or equivalent to the base of the primary slipface/precipitation ridge lee slope. This last limit was used as an index in this study to qualify the landward migration rate of the dune. Rates were

negative (positive) landwards (seawards). Extraction of L_{df} and L_{wl} positions in each image was performed along seventy 50-m spaced shore-normal transects (on average of 8 profiles per area box). Positions were estimated to within a total error under +/-5 m at maximum (Table 1), which is suitable to investigate large dunefields with typical migration rates of 10's to 100's of meters. This range reflects errors due to inherent inaccuracies of the base map, photograph referencing and measurement errors and is similar to that reported in the literature (Gonzalez-Villanueva et al., 2013; Gao et al., 2021). Furthermore, the vegetated dune was mapped but its percentage of surface is not given due to uncertainties of the manual method, the quality of the photographs or the difficulty of determining it accurately in a context of dune destabilization. Nevertheless, this allows us to understand the main trends of its evolution.

4.2 Ground-Penetrating Radar data

The detailed internal structures of the Trencat coastal dune system was surveyed using a Mala ProEx system with a series of two antennae with center frequencies of 100 and 500 MHz. GPR antennas were coupled with survey wheel and a Trimble R6 RTK-GPS to geo-locate and record the topography, providing for geo-positioning at centimeter-scale accuracy in three dimension. Antennas have different depths of penetration and resolution (30 cm and 6 cm resolutions for the 100 and 500 MHz antennae, respectively). Each GPR sections were collected by both antennae along three cross-shore transects (CS-1 to CS-3, Figure 1c) showing a complete section through the dune and three longshore transects (LS-1 to LS-3). Data were processed (time-zero drift, background removal, band-pass filtering, amplitude correction) using ReflexW Software and topographically corrected using RTK-GPS data. The velocity used to calculate the time-depth conversion depth was 0.14 m/ns, a value that has been determined from common mid-point (CMP) method during the field campaign by two 500 MHz antennae. After processing, the GPR images were interpreted on the basis of radar facies identified on the profiles following the concepts of Neal (2004). Signal is not especially disturbed by the water table neither salt water intrusion, excepted from the upper beach part. The GPR transects used herein are the 500 MHz profiles CS-3 and LS-1 which illustrate the dune area with more detail than 100 MHz profiles. The objective is not to detail precisely the internal architecture of each groupe of reflectors imaged by the radargram but illustrate the internal complexity of this system and the amplitude of evolution.

4.3 Topographic data from 2005 to 2020

Several airborne LiDAR data (8 campaigns) were also used in order to analyze morphological and sand budget evolution over the last 15 years (2005, 2011, 2014, 2016, 2017, 2018, 2019,

2020). All campaigns were conducted in autumn apart from the 2011 campaign that took place in winter. It allows interannual comparisons and limits seasonal biase. The generated datasets have been acquired in the framework of OCA (see Bossard and Nicolae Lerma, 2020, for technical details). All data sets were controlled using 1550 DGPS point measured in unobstructed and flat surfaces. Comparisons emphasizes an altimetric error inferior to 0.2 m and generally near to 0.1 m (Table 1). The generated DTMs were 1 m horizontally gridded in the French official topographic reference NGF/IGN69. The topographic evolution of the foredune, transgressive dune and landward dune of each area (N_2 to N_7) were calculated between each survey date. These variations are expressed both in terms of total volume (m^3/year) and in volume per beach width (m^3/m/year) to address the alongshore variability.

4.4 Wind data

Wind data were analyzed from a meteorological station located at Cap-Ferret, 15 km north of the study site (Figure 1a). The data cover the period from 1973 to 2021, with a notable gap between 1992 and 1998. The wind data were analyzed (in m/s) to obtain aeolian sediment drift potentials following the method proposed in Fryberger and Dean (1979) and Miot da Silva and Hesp (2010). The method uses wind speed and direction data to calculate the potential sand transport. Drift Potentials (DPs) for each class of velocity and direction are produced to create a sand rose, and the resultant sand drift potential (RDP) indicates the net direction of aeolian transport and its magnitude. Methodological steps and potential errors are discussed by Fryberger and Dean (1979), Arens (1997), Bullard (1997) and Pearce and Walker (2005). Following the Fryberger and Dean (1979) model, a grain size with the median (D_{50}) of 0.3 mm and a threshold velocity of ~6.17 m/s was assumed in the DP and RDP calculations. The threshold velocity was calculated following methods in Zingg (1953) and Belly (1964).

5 Results

5.1 Chronology of historical changes

The historical aerial photographs covering 75 years (1945-2020) enabled the identification of three primary evolutionary stages of the Trencat coastal dune system based on the dune migration index (L_{wl}): 1) a rapid landward migration of the dune (1945-1959, Stage I); 2) a slow or no migration together with a strong eolian deflation of the dune stoss slope (1959-2000, Stage II); and 3) another landward migration of the dune associated with the development of a new foredune (2000-2020, Stage III). These three distinct stages are analyzed below. We

recognize that the duration of stages is constrained by the aerial photographs dataset, therefore, the years of stage divisions are not exactly the same as the years of used aerial imagery.

Stage I – Rapid landward migration (1945-1959): Stage I is characterized by a strong landward migration of the transgressive dune (L_{wl}) during the 1945-1950 period by up to 115 m $^{+}/_{-}$ 10 m (-23 m/year) in zone N_5 (Figure 3, Table 2). While the northern part (M_1 to N_5) exhibits a relative stability between 1950 and 1959, the southern zones (N_6 to M_8) continue to migrate landwards with a displacement of up to 50 m $^{+}/_{-}$ 10 m (-5.8 m/year) in N_7. During this stage, the dynamics of the dune foot (L_{df}) is stable or in erosion in the northern part (M_1 to N_3) (Table 2). The landscape is covered by a low density of vegetation only in the north in 1945 (Figure 3). The vegetation colonization and partial stabilization on the southern parts of the dune system between 1950-1959 is due to human intervention. Interpretation of each aerial photograph suggests that the system is composed by a unique dune.

Stage II – Little to no landward migration and strong eolian deflation of the transgressive dune (1959-2000): Stage II indicates that over 40 years there is almost no or slow dune migration (L_{wl}). However, this stage is punctuated by strong morphological evolution due to aeolian deflation (Figure 3, Table 2). Between 1959 and 1964, a dense vegetation coverage is observed across most of the upper part of the dune (relatively flat areas). This is also observed during the periods 1964-1968 and 1973-1979 in the managed zone M_8, which is due to intensive marram planting by dune managers. Furthermore, from the mid-1970s until today, destabilization of the dune by eolian erosion is observed. This concerns initially the southern zone (N_5 to N_7), then all the system, even if the northern parts (N_2 and N_3) are less affected. This leads to the formation of many blowouts and breaches where only densely vegetated areas are preserved. Between 1979 and 1982, the evolution of the system is characterized by a new strong landward migration of the dune on N4, by slipface or precipitation ridge advance, by 69 m $^{+}/_{-}$ 10 m on average (-23.7 m/year) (Table 2). It is only during this short period and on local area that a significant dune migration (L_{wl}) is observed during Stage II. The erosion of the system seems to accelerate on several areas from the 1990s onwards, as evidenced by the strong decrease of the vegetated surfaces (Figures 3 and 4).

During this stage, the dune foot (L_{df}) shows that accretion occurred between 1959 and 1968 in the northern part of the dune (M_1 to N_5), then in the southern part (N_4 to M_8) between 1968 and 1973 (Table 2). The year 1968 is the beginning of a long period of erosion starting in the north (M_1 to N_2) then progressing southwards during the following years. This erosion impacted the

northern part until 1996 and the southern part until 2005. Erosion rates are large, often greater than -5 m/year $^{+}/_{-}$ 2 m and locally exceeding -10 m/year $^{+}/_{-}$ 2 m at several periods. Interpretation of each aerial photograph suggests that the system is again composed by a unique dune.

Aeolian drift potential (DP) and resultant drift potential (RDP) were relatively high in the 1973 to 1979 period, and then declined towards 1991 (Figure 5). A poor correlation is found between the highest potential sand transport shown in the record (1973 to ~1979) and dune migration (1979-1982). Note, however, there will be significant topographic acceleration of wind flow up this relatively steep, high transgressive dune (cf. Hesp and Hyde, 1996).

Stage III – Moderate landward migration and strong aeolian deflation of the dune (2000-2020): Stage III corresponds to a new landward migration phase of the dune (L_{wl}) which is observed in each photograph, except in the managed zones (M_1 and M_8) (Table 2). The 2005-2009 period seems to be the most dynamic for the northern zone (N_2 to N_5) with a migration of approximately 30 m $^{+}/_{-}$ 5 m (-3 to -10.6 m/year), while the 2016-2020 period is slightly more dynamic in the southern part (-5.7 to -6.3 m/year). In the northern zone (N_2 and N_4), the landward migration seems to slow down or stop since 2009. During Stage III, the position of the dune foot (L_{df}) continues its seaward progradation from north to south as observed since 1996. This progradation together with an assessment of vegetation coverage indicates the development of a new foredune along the backshore in the early 2000's in the north, and then in the mid-2000s in the south (Figure 3). A period of strong erosion of the dune foot is observed on the southern part (N_5 to N_7) during the period 2009-2016 in relation with the very energetic 2013-2014 winter (Castelle et al., 2015) that had a stronger impact in the south than the northern part (M_1 to N_4).

Potential aeolian transport (total DP or RDP) is relatively low throughout the 2001 to 2018 period (Figure 5). However, the wind regime is energetic enough to move sand and cause significant erosion of the entire seaward face of the transgressive dune field and a significant downwind deposition across the dune crest and lee slopes.

To summarize, the 75-year analysis of the Trencat dune shows an evolution from a single transgressive dunefield to a system composed of a foredune and a transgressive dunefield (Figure 6). Over this period, L_{wl} migration increases southwards, from 33 to 233 m $^{+}/_{-}$ 7.5 m (i.e. -0.4 m/year to -3.1 m/year on average) for N_2 to N_7, respectively (Figure 6c). In comparison, the managed zones (M_1 and M_8) show only little landward migration (0.1 to 0.4

m/year for M_1 to M_8)). At the beach-dune interface, L_{df} evolved according to a north-south gradient, with a seaward progradation in the north (M_1 and N_2), stability in the central part (N_3 and N_4) and retreat in the south (N_5 to M_8). The coupling of these dynamics leads to a widening of the dune system (Figure 6c) except in M_8 due to an erosion of the dune foot and a weak landward migration due to management actions, and an overall anticlockwise rotation of the system from NNE to N (Figure 6a,b).

5.2 Internal architecture of the dune system

The GPR surveys depict the stratigraphic framework of the dune through 15 m depth (Figures 7 and 8). Topographic profiles surveyed between 2005 and 2021 are superimposed onto the GPR profiles to understand the chronostratigraphic evolution of this transgressive dune. Reflectors within the transgressive dunefield are in line with the topographic profiles. Data shows that the transgressive dune migrated landward over paleosols which are identified in all radar profiles as high-amplitude reflectors (Figure 7). One of them, the upper most, is located near 8-9m NGF which is well correlated with field observations of the outcrops. Above the upper paleosol, cross-shore profile CS-3 show three distinct sectors (Figure 7): (1) From the upper beach to cross-shore position $X \approx 75$ m, the foredune, which has been growing for the last 10 years and which elevation is now reaching up to 10-13 m NGF. The foredune internal architecture indicates a steepening of the relief during vertical growth; (2) The central part of the cross-shore profiles shows the dune erosion section (essentially stoss face deflation). Indeed, on CS-3 a surface of erosional truncation on the ground cuts off landward dipping reflectors constituting the former dune (X= 75 to 300 m). The altitude of the deflation plain (X= 100 m to 200 m) corresponds to the outcrop of the a paleosol at 8m NGF; (3) Landward, the dune internal architecture reflects a landward migrating transgressive dune system, with steep landward dipping (slipface/precipitation ridge) reflectors (18-26°) with downlap terminations in contact with the upper paleosol.

Even if cross-shore profiles show similarities alongshore, the alongshore GPR transects in the transgressive dune reveal a dramatic alongshore variability (Figure 8). Such variability reflects a strongly 3D dynamics of the dune migration owing to local disparities of the former morphology and plant cover, leading to areas with greater erosion (blowouts, deflation plain, remnant knobs) and lateral deposits associated with these structures. From the north to the south, this alongshore profile may be divided into 5 parts corresponding to spatial area of

concordante comportement. The part 1, from *Y*= 0 to 50 m (part 1), is defined by northward dipping reflectors with steeply sloping (12-16.5°). The filling of a scour surface (former blowout) (*Y*= 60-120 m, part 2) is identified by concave-up reflectors followed by 50-m wide and 2-3-m thick aggradational strata. The third part (*Y*= 120 to 270 m) is characterized by three ridges where reflectors are relatively horizontal with erosional truncations on each side except for the northernmost face. To the south, up to *Y*= 375 m, the dune is defined by horizontal or low angle reflectors from the paleosol to 12-14 m NGF, and are overlaid by steep northward dipping reflectors (17.5°). Finally, the southern part of the profile is defined by southward dipping reflectors (*Y*= 400 to 550 m) with steep slopes (up to 19,5°) to more gentle slopes with slightly convex-downward strata (*X*= 550 to 650 m). The longshore GPR data indicates that the upper part of the profile was modified between 2005 and 2011 but also before 2005 during stage II.

5.3 Focus on dunefield sediment budget during Stage 3 (2005-2020)

The most recent period (2005-2020) is analyzed in terms of volumetric changes based on airborne LiDAR focusing on N_2 to N_7. (Figures 9 and 10). The analysis of each survey shows that this sector exhibits a systematic increase of sediment volume, although with some time variability (Figures 9 and 11). The most rapidly evolving period was 2005-2011 with a gain of 105,000 m^3/year (46 m^3/m/year) (Figure 11a,b). During the period 2011-2016, beaches suffered from the energetic storms of the 2013-2014 winter, causing substantial beach and dune foot erosion. Despite the observed erosion, the overall 2011-2014 sediment budget is positive (46,000 m^3/year). The 2014-2016 period was characterized by beach recovery, and sediment transfer to the dune was reduced (11,000 m^3/year) in comparison with previous and subsequent periods (Figure 11a). Between 2016 and 2020, a gain of sediment of 40,000 m^3/year to 90,000 m^3/year (20 to 39 m^3/m/year) is observed. Overall, the northern sectors show an increase in sediment volume greater than in the southern sectors between 2005 and 2016 (Figure 11f). This behavior seems less marked over the more recent period (2016-2020).

The volumetric changes of the foredune and the transgressive dune reveal a strong longshore variability. A new foredune developed first in the north (2005) to then to the south (2016) (Figures 9 and 11j). From 2016-2017, the foredune is well established along the entire field site and its gain of sediment is relatively similar for all areas (between 20 and 25 m^3/m/year on average between 2016 and 2020) except in zone N_4 (11 m^3/m/year, Figure 11j). The presence of the foredune implies a reduction in sediment supply to the landward transgressive dune. This

is verified during the period 2005-2011, when a gain of 24-31 m^3/m/year in the north is approximately twice as less than which occurred in the south (N_6 to N_7) where there is no foredune (Figure 11h). This behavior is also observed on the N_6 and N_7 areas over 2005-2011 (100% of transfer to the dune) and 2019-2020 (50% of transfer to the dune) for a similar sediment supply from the beach (Figure 11f,h,j).

To summarize the 15 years of 3D survey, the dune system gained more than 1 million m^3 +/- 250,000 m^3 of sediment (30 m^3/m/year). The gain per unit area decreases from north (42 m^3/m/year) to south (24 m^3/m/year) (Figure 11b,d and Table 3). The evolution of the foredune, which is wider and slightly higher in the north than in the south in relation to its age of development, represents a significant portion of this gain, with an increase of 394,000 m^3 +/- 68,000 m^3 of sediment. The gain of the transgressive dune represents 673,000 m^3 +/- 190,000 m^3 (Table 3). It is the southern part (N_6 to N_7) which has the largest volumetric gain (21 to 27 m^3/m/year). These changes, coupled with the stoss slope erosion/deflation of the transgressive dune, result in an average elevation of the transgressive dune increasing by about 1 m in 15 years (Table 3).

5. Morphodynamics of the Trencat Transgressive Dunefield System

This study describes the 75-year evolution of a transgressive dunefield revealing two periods of rapid landward migration (1945-1959 and 2000-2020), separated by a ~40 year reasonably stable period or low migration (1959-2000) (Figure 12). The onset of Stage II (1959) coincides with a dune undergoing vegetation colonization and partial stabilization due to human intervention on the southern parts of the dune system between 1950 and 1959 (Figures 3 and 12). The sediment transported across the dune foot was trapped by vegetation leading to its stabilization and aggradation rather than migration (cf. Hugenholtz & Wolfe, 2005; Yizhaq et al., 2007; Arens et al., 2013). On the downdrift side of Arcachon inlet (approximately 4-6 km updrift of the field site; Figure 1), a large shoal welding event occurred between 1957 and 1959 (Figure 2) (Michel et al., 1995). This welding induced a large widening of the beach updrift of the study site, with the bulge of sand (also known as a sandwave, cf. Thevenot and Kraus, 1995; Davidson-Arnott and Van Heyningen, 2003; Ribas et al., 2013) subsequently migrating downdrift towards the study site. Downdrift of the sandwave (i.e the field site), an intense and persistent erosion of the dune foot was observed at M_1-N_2 from 1968, N_3 from 1973 and then

gradually in the southernmost parts from 1982 (Table 2b). The erosion of the dune foot appears to intensify as the sandwave approaches and the shape of the bulge is at a maximum, notably from 1991. This behavior has been observed elsewhere, when the geometry of the sandwave disturbs the littoral drift and reduces the sediment supply (Davidson-Arnott and Van Heyningen, 2003; Robin and Levoy 2007; Robin et al., 2009, 2020a). This resulted in the development of dune scarping, blowouts, a large deflation basin and ramp, and a reduction in the extent of vegetated surfaces from the end of the 1970's (Figures 3, 4, 12). This system destabilization, toward a more erosional morphological state, stimulated dune cannibalization and translation of the transgressive dune, likely with concurrent elevation of the dune crest due to the presence of a patch of residual vegetation located mainly on its upper part, but no migration is observed (Figures 3 and 4). It is also observed on LS-1 with high amplitude of topographic evolution in longshore orientation (Figure 8). This phase lasted almost 30 years due to the slow diffusion and downdrift migration of the sandwave. Since 1996, the gradually diffused sandwave resulted in substantial sediment supply in the northern part of the study area (cf. Davidson-Arnott and Van Heyningen, 2003), attested by the initiation of a new foredune since 2000 in M1, and then gradually in the southernmost part (Figure 12). The erosional morphological state associated with sparse vegetation cover on the upper part of the dune and new sediment input created conditions for the transfer of large quantities of sediment to the upper part of the dune, since 2000, and drove its cannibalization and migration between 2000 and 2005 (Stage III).

However, the dune has a longshore variability as shown by southern parts which migrate faster than northern part (Figure 6). This is explained by a higher density of vegetation and the complex morphology of the north part of the dune (M_1, N_2 and N_4 (Figure 3)) which does not allow the establishment of a long and wide ramp (or deflation basin) to promote the transfer of sediment on the slipface/precipitation ridge lee slope as observed elsewhere (Hesp, 2013a; Ollerhead et al., 2013). These differences are already observed on the 1945 photography (Figure 3). Figures 7 and 10 clearly illustrate that different portions of the dunefield respond in numerous ways over time to external and local forcing factors. It is common to see different portions of transgressive dunefields migrating faster in some areas compared to others (cross-shore but also alongshore (Figure 8)), and piling up in some places compared to advancing landwards as a function of vegetation cover, degree of forest/vegetation on the slipface and precipitation ridge, local wind and topographic factors, and local sand supply (e.g. Martinho et

al., 2010; Hesp et al., 2011). The Trencat system provides further documentation of this alongshore variability in dunefield morphodynamics.

6 Discussion

6.1 Dune remobilization: Internal vs external factors

The Trencat dune behavior is characterized by a new remobilization stage post-2000 after a long reasonably stable stage (Figure 12). This is contrary to most of the multi-decadal coastal dune studies showing increased stability by enhanced vegetation cover, without a destabilization stage (Martinho et al., 2010; Provoost et al., 2011; Jackson et al., 2019a; Pickart and Hesp, 2019; Gao et al., 2020, 2021). Given that the field site has been in an unmanaged evolution at least since the end of the 1950's, it is possible to address the role of internal and external factors on its evolution. Despite the statistically significant increase in storminess and incident winter wave energy over the last decade in the northeast Atlantic, there is no large-scale climate pattern of atmospheric variability that could explain this 3-stage behavior at Trencat (Castelle et al., 2018). Moreover, additional windblown sand transport analysis (Figure 5) indicates that there is no clear variability that could explain such changes in dune dynamics. Anthropogenic factors such as the influence of military activities since the end of the 1950's may have potentially contribute to the changes of the morphological state of the dune in some places (Rickard et al., 1994; Thompson and Schlacher, 2008), although these activities are to an extent impossible to quantify here, and are considered to be minor. Despite some uncertainties due to the image resolution and the difficulty of mapping vegetation cover on a destabilized dune system, orthophoto inspection indicates that the decrease in vegetation cover at the end of the 1970's resulted from erosion of the dune foot which begins in 1968 in the northern parts. It led to aeolian deflation and the destabilization of the system as previously noted (Figure 12). This erosion seems to be linked to the approaching updrift sandwave disturbing the longshore sediment drift. This process confirms the importance of combining cross-shore and longshore transport processes in long-term beach (Vitousek et al., 2017; Robinet et al., 2018) and beach-dune evolution models (Cohn et al., 2019, Hallin et al., 2019a, b; Moulton et al., 2021). Mathew et al., (2010) show that a severe storm can induce large scale erosion and overwash further triggering a transgressive dune stage or phase. Sustained foredune (dune) erosion is also a factor mentioned in the literature (Pye, 1990; Jackson et al., 2019b) but little actual proof or evidence of this has been documented (Hesp, 2013a). Instead, Hesp et al.,

(2022) show that foredune erosion did not result in dunefield formation, but in similarity to observations shown in this study, scarping of a high relict vegetated dunefield and subsequent cannibalization did produce a new transgressive dunefield. Our results indicate that the remobilization period of the transgressive dune system stage is not especially driven by external factors (e.g. wind, waves), although once deflation begins on the stoss face of the transgressive dunefield post-2005, it is self-sustaining and wind is important in this. Instead, the welding of swash bars on multi-year or multi-decadal timescales, i.e. factors internal to the estuary inlet system are hypothesized to assist in the onset of the last active dunefield stage along this stretch of coast. The behavior has not been observed elsewhere in southwest France as, on most of the Aquitaine coast, contemporary coastal dune morphology and changes are strongly controlled by human fixation actions (Bossard and Nicolae Lerma, 2020; Robin et al., 2021). The emblematic transgressive Pilat dune (located at few km north the field site) persistently migrates inland, and a stable stage has never been observed probably due to the absence of vegetation and management actions. However, in the context of present and future sea-level rise, an increase in wave and wind energy, and intensification of coastal erosion, this study provides some information on how freely evolving dune systems with sufficient aeolian energy, sand material and available transfer area could evolve in the future.

6.2 Dune remobilization: Time scale

Geomorphological changes are complex because several parameters can influence dune mobility differently according to their magnitude (Provoost et al., 2011). The mechanisms underlying the onset of stage II and III discussed in the previous section have similarities with the Jackson et al. (2009b) conceptual model applied to the last major phase of dune mobility in Europe during the LIA. This study provides a time frame, although specific to the study site, and shows the relative speed with which transgressive dunefield change takes place. It is thus observed that the dune is influenced by the shoal welding event of 1959 which began 4-6 km updrift from the study area and impacts dune morphodynamics even 70 years later. This historically long time scale is also observed by Mathew et al. (2010). The perturbation induced by the erosion of the dune foot from 1968 in the northern section, is not synchronous with the beginning of the decline in vegetation cover observed since the end of the 1970's. Similarly, the beginning of destabilization of the system is not synchronous with the start of remobilization observed in 2000 suggesting a threshold value of vegetation cover to induce sufficient sediment availability for a significant inland migration. The vegetation decline observed in the field site occurs over a long period (1979-2000), in relation to hysteresis curves

described by Tsoar (2005). Once vegetation is established and dune systems stabilize (1959-1968, stage II), destabilization requires much more energy to induce vegetation destruction by wind stress and sand movement, than the fixation. This non-synchronization between perturbation and consequence can reach several years or decades in our study and can be referred to as a relaxation time expected for a morphodynamic system to adapt and lead to significant change (Hugenholtz & Wolfe, 2005; Galiforni-Silva et al., 2020). Sufficiently long consideration of the key factor(s) influencing a dune system before an identified morphological response is then recommended. So, the trigger of the remobilization is influenced by the intensity of the perturbation, but also its duration.

6.3 Sediment supply across the foredune-transgressive dune system and initiation of a new foredune

Historical analysis by aerial photographs since 1945 shows a landward dune migration increasing southwards, from 33 to 233 m in 75 years (Figure 6). It is notable that almost the entire volume of the 1945's dune was remobilized during this migration by rollover or translation (Figure 7). The forest boundary identified in the 1945 photograph has been covered by the landward migration of the transgressive dune and appears today in the form of a paleosol and shrubby detritus on the stoss slope (Figure 7). In contrast to the foredune literature, knowledge about elevation variations by DEM's of transgressive dunefields are scarce. Gonzalez-Martin and Rodriguez-Santalla (2021) observed a gain of 52% between 2008 and 2015. However, Perez-Albertini et al., (2021) identified an erosion of -110,317 m^3 due to high anthropogenic influence. The more recent 2005-2020 period allows a quantification of volumetric changes. Although the dune system has significantly cannibalized itself coupled with the formation of the new post 2005 foredune, it has grown by approximately 673,000 m^3 $^{+}/_{-}$ 190,000 m^3 in the unmanaged area with some alongshore and temporal variations (Figures 8 and 10, Table 3). It represents 24 % of the 2005 dune system taking the altitude of the upper paleosol identified by GPR as the base of the dune (Figure 7). Such large sediment transfers have also been observed by Pickart and Hesp (2019) when the foredune was generally flatter, wider and less vegetated, or during stormy conditions. This also confirms that the landward sand transport over the crest of the foredune, often quantified at the process scale, potentially represents large volumes of sediment delivery to landward dunes on the decadal scale (Davidson-Arnott and Law, 1996, Christiansen and Davidson-Arnott, 2004). However, here the formation and aggradation of the new foredune disturbed the supply from the upper-beach

to the dune, capturing a large amount of windblown sand (394,000 m^3 +/- 68,000 m^3 between 2005 and 2020). This process is well illustrated in the N_6 and N_7 areas for the periods 2005-2011 (100% of transfer to the dune) and 2019-2020 (50% of transfer to the dune) for a similar sediment supply from the beach (Figure 11f,h,j). Thus, it is likely that as the foredune widens and becomes more vegetated, coupled with the increasing downwind remoteness of the transgressive dune and deflation basin extension, the transgressive dunefield becomes decoupled from the beach-foredune portion of the system. This evidence of the morphodynamics of the transgressive dunefield can inform understanding regarding current research on Nature Based Solutions applied to dunes following their "re-mobilisation" (Castelle et al., 2019; Delgado-Fernandez et al., 2019). It is shown here that the storage of a large sediment volume inland occurs while a new foredune is created, and illustrates how it evolved over time, at least during the first two decades.

Our results suggest that the post-2005 foredune formation is favored by a moderate to high sediment supply during this period. Its position on the backshore of the supratidal zone can take two different paths. In some locations (M_1, N_2, N_4), the incipient foredune formed against the (vegetated) dune, and subsequently developed by progradation, i.e. leading to a seaward development as observed in many other coastal environments or during beach-dune recovery (Hesp, 2013b; Pellon et al., 2020; Robin et al., 2020b, 2021). In contrast, in some locations (N_5, N_6, N_7), the incipient foredune formed well seaward of the (unvegetated) dune (Figures 7 and 10) and subsequently slowly migrated landwards. However, the evolution of the foredune is mainly accomplished by vertical accretion. Migration of the dune leads to the presence of a deflation basin whose altitude coincides with the location of a paleosol at 8-9 m NGF (Figure 7), becoming increasingly larger resulting in complete decoupling of the foredune and transgressive dune (Hesp, 2013a; Pickart and Hesp 2019). This new accommodation space seems to explain the building pattern of the foredune, compared to the northernmost part.

Conclusion

This study was based on a holistic approach providing fresh and quantitative insight into transgressive dunefield behavior. The combination of GPR, historical photographic imagery, and LiDAR surveys clearly illustrates the historical evolution of the transgressive dunefield and foredune system both across- and alongshore. Three major periods based on migration rate may be distinguished in the modern dunefield, namely, Stage I (1945-1959, up to 10 m/year,

reaching 23 m/year in N_5) where rapid migration occurred, Stage II (1959-2000) which was mostly characterized by low to no migration but strong morphological evolution, and Stage III (2000-2020, 1-6 m/year) characterized by significant seaward deflation, vertical crest accretion, and moderate landward migration. The onset of stage II is due to the fixation of vegetation by human action between 1950 and 1959 inducing a stabilization of the system until 1968. The remobilization during the stage III is hypothesized to be driven by long and sustained upper backshore/dune toe erosion beginning in 1968, inducing destabilization of the dune and erosion of the vegetation cover over some decades. Our results indicate that the trigger of the remobilization is influenced by the intensity and duration of the perturbation, but also the long period on the erosional morphological state that occurred. The destabilization period is not especially driven by external factors (e.g. wind, waves) but is attributed to a large-scale ebb shoal welding updrift of the study site disturbing the longshore sediment supply, i.e. factors internal to the estuary inlet system. Therefore, this study shows that the natural remobilization of a transgressive dunefield can be induced by dune foot erosion.

Although the dune system has significantly cannibalized itself, especially post-2005, the transgressive dunefield has also grown in volume by about 673,000 m^3 +/- 190,000 m^3 during the 2005-2020 period. It represents 24 % of the 2005 dune system. The formation of the post-2005 foredune (394,000 m^3 +/- 68,000 m^3) is linked to the high to moderate sediment supply and accommodation space available due to the landward migration of the transgressive dune. Sand supply from the beach to the dunefield is therefore still significant but lower, and shows that in some cases at least the presence of a relatively substantial foredune does not result in a termination of landward dunefield dynamics. In the context of present and future sea-level rise, an increase in wave and wind energy, and intensification of coastal erosion, this study provides some information on how freely evolving dune systems with sufficient aeolian energy, sand material and available transfer area could evolve in the future.

Acknowledgements

T-REX project was funded by Observatoire de la Côte Nouvelle Aquitaine (OCNA). Stuart Lane and two anonymous reviewers provided salient suggestions for improvement of the manuscript.

Data availability statement

The data used in this study are available upon request to authors.

Conflict of interest statement

The authors declare that they do not have any conflict of interest.

References

Aagaard, T., Davidson-Arnott, R.G.D., Greewood, B. & Nielsen, J. (2004). Sediment supply from shoreface to dunes – linking sediment transport measurements and long term morphological evolution. *Geomorphology*, 60, 205-224.

Arens, S.M. (1997). Transport rates and volume changes in a coastal foredune on a Dutch Wadden Island. *J. Coast. Conservation*, 3, 49–56.

Arens, S.M., Slings, Q. L. & de Vries, C. N. (2004). Mobility of a remobilized parabolic dune in Kennemerland, The Netherlands. *Geomorphology*, 59, 175-188.

Arens, S.M., Mulder, J. P. M., Slings, Q. L., Geelen, L. H. W. T. & Damsa, P. (2013). Dynamic dune management, integrating objectives of nature development and coastal safety: examples from the Netherlands. *Geomorphology*, 199, 205-213.

Barchyn, T. E. & Hugenholtz, C. H. (2013). Reactivation of supply-limited dune fields from blowouts: A conceptual framework for state characterization. *Geomorphology*, 201, 172-182.

Belly, P.Y. (1964). Sand movement by wind. U.S Army Corps of Engineers, CERC, Washington, DC. Tech. Memo. 1, 38.

Bossard V. & Nicolae Lerma A. (2020). Geomorphologic characteristics and evolution of managed dunes on the South West Coast of France. *Geomorphology*, 367, 107312.

Botha, G. A., Bristow, C. S., Porat, N., Duller, G., Armitage, S. J., Roberts, H. M. & Schoeman, P. (2003). Evidence for dune reactivation from GPR profiles on the Maputaland coastal plain, South Africa. *Geological Society, London, Special Publications*, *211*(1), 29-46.

Bullard, J.E. (1997). A note on the use of the Fryberger method for evaluating potential sand transport by wind. *J. Sed. Res,* 67 (3A), 499–501.

Burvingt, O., Lerma, A.N., Lubac, B., Mallet, C. and Senechal, N. (2022). Geomorphological control of sandy beaches by a mixed-energy tidal inlet. *Marine Geology*, 450, 106863.

Buynevich, I., Bitinas, A. & Pupienis, D. (2007). Reactivation of coastal dunes documented by subsurface imaging of the Great Dune Ridge, Lithuania. *Journal of Coastal Research*, 226-230.

Buynevich, I. V., Souza Filho, P. W. M. & Asp, N. E. (2010). Dune advance into a coastal forest, equatorial Brazil: a subsurface perspective. *Aeolian research*, *2*(1), 27-32.

Castelle, B., Bourget, J., Molnar, N., Strauss, D., Deschamps, S. & Tomlinson, R. (2007). Dynamics of a wave-dominated tidal inlet and influence on adjacent beaches, Currumbin Creek, Gold Coast, Australia. *Coast. Eng*, 54, 77e90.

Castelle, B., Marieu, V., Bujan, S., Splinter, K.D., Robinet, A., Sénéchal, N. & Ferreira, S. (2015). Impact of the winter 2013-2014 series of severe Western Europe storms on a double-barred sandy coast: Beach and dune erosion and megacusp embayments. *Geomorphology*, 238, 135-148.

Castelle, B., Dodet, G., Masselink, G. & Scott, T. (2017). A new climate index controlling winter wave activity along the Atlantic coast of Europe: The West Europe Pressure Anomaly. *Geophysical Research Letters*, 44, doi: 10.1002/2016GL072379.

Castelle, B; Dodet, G; Masselink, G. & Scott, T. (2018). Increased winter-mean wave height variability, and periodicity in the northeast Atlantic over 1949-2017. *Geophysical Research Letters*, 45, 3586-3596.

Castelle, B., Laporte-Fauret, Q., Marieu, V., Michalet, R., Rosebery, D., Bujan, S., Lubac, B., Bernard, J.-B., Valance, A. Dupont, P., Ould El Moctar, A. & Narteau, C. (2019). Nature-Based Solution along High-Energy Eroding Sandy Coasts: Preliminary Tests on the Reinstatement of Natural Dynamics in Reprofiled Coastal Dunes. *Water*, 11, 2518.

Christiansen, M.B. & Davidson-Arnott, R. (2004). Rates of landward sand transport over the foredune at Skallingen, Denmark and the role of dune ramps. *Geografisk Tidsskrift, Danish Journal of Geography*, 104 (1): 31-43.

Clemmensen, L. B., Bjornsen, M., Murray, A. & Pedersen, K. (2007). Formation of Aeolian dunes on Anholt, Denmark since AD 1560: a record of deforestation and increased storminess. *Sedimentary Geology*, 199, 171-187.

Cohn, N.; Hoonhout, B.M., Goldstein, E.B. & De Vries, S. (2019). Exploring marine and Aeolian controls on coastal foredune growth using a coupled numerical model. *J.Mar Sci ENg*, 7, 1-25.

Costas, I., Reimann, T., Tsukamoto, S., Ludwig, J., Lindhorst, S., Frechen, M., Hass, H.C. & Betzler, C. (2012). *Quaternary Geochronology*, 10, 16-23.

Costas, S., Alejo, I., Rial., Lorenzo, H. & Nombela, M.A. (2006). Cyclical evolution of a modern transgressive sand barrier in northwestern spain elucidated by GPR and aerial photos. *Journal of Sedimentary Research*, 76, 1077-1092.

Davidson, S. G., Hesp, P. A. & Miot da Silva, G. (2021). Rapid shoreline erosion and dunefield change, Salmon Hole, South Australia. *Science of the Total Environment*, 767, 145406.

Davidson-Arnott, R.G.B. & Law, M.N. (1996). Measurement and prediction of long-term sediment supply to coastal foredunes. *Journal of Coastal Research*, 12, 654-663.

Davidson-Arnott, R.G.B. & Van Heyningen, A.G. (2003). Migration and sedimentology of langshore sandwaves, Long Point, Lake Erie, Canada. *Sedimentology*, 50, 1123-1137.

Delgado-Fernandez, I., Davidson-Arnott, R. & Hesp, P.A. (2019). Is "re-mobilisation" nature restoration or nature destruction? A commentary. *Journal of Coastal Conservation*, 23, 1093-1103.

Fillon, L. (1984). A relationship between dunes, fire and climate recorded in the Holocene deposits of Quebec. *Nature*, 309, 543-546.

Froidefond, J.M. & Prud'homme, R. (1991). Coastal erosion and aeolian sand transport on the Aquitaine coast. *Acta Mechanica*, Suppl.2, 147-159.

Fryberger, S.G. & Dean, G. (1979). Dune forms and wind regime. *In: McKee, E.D. (Ed.), A Study of Global Sand Seas : Geol. Survey Prof. Paper, 1052. US Govt. Printing Office, Washington*, pp. 137–170.

Galiforni-Silva, F., Wijnberg, K.M. & Hulscher, S.J.M.H. (2020). On the relation between beach-dune dynamics and shoal attachment processes: A case study in Terschelling (NL). *Journal of Marine Science and Engineering*, 8, 541.

Gao, J., Kennedy, D.M. & Konlechner, T.M. (2020). Coastal dune mobility over the past century: A global review. *Progress in Physical Geography: Earth and Environment*, 44(6), 814-836.

Gao, J., Kennedy, D.M., Konlechner, T.M., McSweeney, S., Chiaradia, A. & McGuirk, M. (2021). Changes in the vegetation cover of transgressive dune fields: A case study in Cape Woolamai, Victoria. *Earth Surface Processus and Lanforms*, 1-15, esp.5284.

Gardner, D.E. (1955). Beach-Sand Heavy-mineral Deposits of Eastern Australia. *BMR Bulletin*, 28.

Girardi, J.D. & Davis, D.M. (2010). Parabolic dune reactivation and migration at Napeague, NY, USA: Insights from aerial and GPR imagery. *Geomorphology*, 114, 530-541.

Gonzalez-Martin, L. & Rodriguez-Santalla, I. C. (2021). Analysis of the dynamics of the Valdevaqueros dune. *Environmental Sciences Proceedings*.

Gonzalez-Villanueva, R., Costas, S., Pérez-Arlucea, M., Jerez, S. & Trigo, R. M. (2013). Impact of atmospheric circulation patterns on coastal dune dynamics, NW Spain. *Geomorphology*, 185, 96-109.

Hallin, C., Larson, M. & Hanson, H. (2019a). Simulating beach and dune evolution at decadal to centennial scale under rising sea levels. *PLoS ONE*, 14 (4): e0215651.

Hallin, C., Huisman, B.J.A., Larson, M., Walstra, D.J.R. & Hanson, H. (2019b). Impact of sediment supply on decadal-scale dune evolution – Analysis and modelling of the Kennemer dunes in the Netherlands. *Geomorphology*, 337, 94-110.

Hesp, P.A. (2011). Dune Coasts. *In: Wolanski E and McLusky DS (eds.) Treatise on Estuarine and Coastal Science*, Vol 3, pp. 193–221. Waltham: Academic Press.

Hesp, P.A. (2013a). Conceptual models of the evolution of transgressive dunefield systems. *Geomorphology*, 199: 138–149.

Hesp, P.A. (2013b). A 34 year record of foredune evolution, Dark Point, NSW, Australia. *Journal of Coastal Research*, SI 65, 1295-1300.

Hesp, P.A., Martinez, M.L., Miot da Silva, G., Rodríguez-Revelo, N., Gutierrez, E., Humanes, A., Laínez, D., Montaño, I., Palacios, V., Quesada, A., Storero, L., González Trilla, G. & Trochine, C. (2011). Transgressive dunefield landforms and vegetation associations, Doña Juana, Veracruz, Mexico. *Earth Surface Processes and Landforms*, 36, 3, 285–295.

Hesp, P.A. & Thom, B.G. (1990). Geomorphology and evolution of transgressive dunefields. *In: Nordstrom, K., N. Psuty and W. Carter (Editors), Coastal Dunes: Processes and Morphology*, 253-288. J. Wiley and Sons.

Hesp, P.A. & Hyde, R. (1996). Flow dynamics and geomorphology of a trough blowout. *Sedimentology*, 43 (3), 505-525.

Hesp, P.A., Da Silva, M., Miot da Silva, G., Bruce, D. & Keane, R. (2022). Review and direct evidence of transgressive aeolian sand sheet and dunefield initiation. *Earth Surface Processes and Landforms*.

Houser, C. (2009). Synchronization of transport and supply in beach-dune interaction. *Progress in Physical Geography*, 33(6), 733-746.

Hugenholtz, C. H. & Wolfe, S. A. (2005). Biogeomorphic model of dunefield activation and stabilization on the northern Great Plains. *Geomorphology*, 70, 53-70.

Idier, D., Charles, E., Mallet, C. & Castelle, B. (2013). Longshore sediment flux hindcast and potential impact of future wave climate change along the Gironde/Landes Coast, SW France. *Journal of Coastal Research*, SI 65, pp. 1785-1790.

Jackson, D. W., Costas, S. & Guisado-Pintado, E. (2019a). Large-scale transgressive coastal dune behaviour in Europe during the Little Ice Age. *Global and Planetary Change*, *175*, 82-91.

Jackson, D.W., Costas, S., Gonzalez-Villanueva, R. & Cooper, G. (2019b). A global "greening" of coastal dunes: An integrated consequence of climate change?. *Global and Planetary Change, 182*, 103026.

Lafon, V., Froidefond, J.M. & Castaing, P. (2000). Méthode d'analyse de l'évolution morphodynamique d'une embouchure tidale par imagerie satellite. Exemple du bassin d'Arcachon (France). *Comptes Rendus de l'Academie des Sciences-Series IIA-Earth and Planetary Sciences*, 331(5), 373-378.

Lafon, V., Froidefond, J.M., Lahet, F. & Castaing, P. (2002). Spot shallow water bathymetry of a moderately turbid tidal inlet based on field measurements. *Remote Sensing of Environment*. 81, 136-148.

Lindhorst, S. & Betzler, C. (2016). The climate-archive dune: sedimentary record of annual wind intensity. *Geological Society of America*, V44; n°9, 711-714.

Marcomini, S. C. & Maidana, N. (2006). Response of eolian ecosystems to minor climatic changes. *Journal of Coastal Research*, 204-208.

Martinho, C. T., Hesp, P. A. & Dillenburg, S. R. (2010). Morphological and temporal variations of transgressive dunefields of the northern and mid-littoral Rio Grande do Sul coast, Southern Brazil. *Geomorphology*, 117(1-2), 14-32.

Mathew, S., Davidson-Arnott, R. G. D. & Ollerhead, J. (2010). Evolution oa a beach-dune system following a catastrophic storm overwash event: Greenwich Dunes, Prince Edward Island, 1936-2005. *Canadian Journal of Earth Sciences*, 47 (3), 273-290.

Mendes, V.R. & Giannini, P.C.F. (2015). Coastal dunefield of south Brazil as a record of climatic changes in the South American Monsoon System. *Geomorphology*, 246, 22-34.

Michel, D., Howa, H. & Tastet, J.P. (1995). Essai de modelisation de l'évolution morphologique d'un banc sableux intertidal (Sud du Bassin d'Arcachon, France). *C.R Acad. Sci. Paris*, t.321, série II a, 497-504.

Miot da Silva, G. & Hesp, P.A. (2010). Coastline orientation, aeolian sediment transport and foredune and dunefield dynamics of Moçambique Beach, southern Brazil. *Geomorphology*, 120: 258-278.

Miot da Silva, G. & Hesp, P.A. (2013). Increasing rainfall, decreasing winds, and historical changes in Santa Catarina dunefields, southern Brazil. *Earth Surface Processes and Landforms*, 38: 1036-1045.

Miot da Silva, G. & Hesp, P.A. (2019). Development of coastal Holocene transgressive dunefields: Examples from South Australia. In *Coastal Sediments 2019: Proceedings of the 9th International Conference* (pp. 1226-1239).

Moulton, M., Hesp, P.A., Miot da Silva, G., Bouchez, C., Lavy, M. & Fernandez, G. (2019). Changes in vegetation cover on the Younghusband Peninsula transgressive dunefields (Australia) 1949 – 2017. *Earth Surface Processes and Landforms*, 44: 459-470. DOI: 10.1002/esp.4508.

Moulton, A.B., Hesp, P.A., Miot da Silva, G., Fernandez, G.B. & Keane, R., (2020). Effects of the increase in vegetation cover and impact of rabbits on the geomorphology of parabolic dunes, Younghusband Peninsula, SA. *J. Coastal Research SI 95*: 50-54.

Moulton, A.B., Hesp, P.A., Miot da Silva, G., Fernandez, G.B. & Keane, R. (2021). Surfzone-beach-dune interactions along a variable low wave energy dissipative beach. *Marine Geology*, 435.

Munoz-Perez, J.J., Navarro, M., Roman-Sierra, J., Tejedor, B., Rodriguez, I. & Gomez-Pina, G. (2009). Long-term evolution of a transgressive migrating dune using reconstruction of the EOF method. *Geomorphology*, 112, 167-177.

Neal, A. (2004). Ground-penetrating radar and its use in sedimentology: principles, problems and progress. *Earth-Science Reviews*. 66, 261-330.

Nicolae-Lerma, A., Bulteau, T., Lecacheux, S. & Idier, D. (2015). Spatial variability of extreme wave height along the Atlantic and channel French coast. *Ocean Engineering*, 97, 175-185.

Nicolae-Lerma, A., Ayache, B., Ulvoas, B., Paris, F., Bernon, N., Bulteau, T. & Mallet, C. (2019). Pluriannual beach-dune evolutions at regional scale: Erosion and recovery sequences analysis along the Aquitaine coast based on airborne LiDAR data. *Continental Shelf Research*, 189, 103974.

Ollerhead, J., Davidson-Arnott, R., Walker, I.J. & Sojan, M. (2013). Annual to decadal morphodynamics of the foredune system at Greenwich Dunes, Prince Edward Island, Canada. *Earth Surface Processes and Landforms*, 38, 284-298.

Oyedotun, T.D.T. (2014). Shoreline Geometry: DSAS as a tool for historical trend analysis. *Geomorphologistical Techniques*, Chapter 3(2.2), British Society for Geomorphology, 1-12.

Pearce, K.I. & Walker, I.J. (2005). Frequency and magnitude biases in the "Fryberger" model, with implications for characterizing geomorphically effective winds. *Geomorphology*, 68, 39-55.

Pedersen, K. & Clemmensen, L. B. (2005). Unveiling past aeolian landscapes: a ground-penetrating radar survey of a Holocene coastal dunefield system, Thy, Denmark. *Sedimentary Geology*, *177*(1-2), 57-86.

Pellon, E., de Ameida, L.R., Gonzalez, M. & Medina, R. (2020). Relationship between foredune profile morphology and aeolian and marine dynamics : A conceptual model. *Geomorphology*, 351, 106984.

Perez-Alberti, A., Gomez-Pazo, A. & Otero, X. L. (2021). Natural and anthropogenic variations in the large shifting dune in the Corrubedo Natural Park, NW Iberian Peninsula (1956-2017°. *Applied Sciences*, 11, 34.

Pickart, A. & Hesp, P.A. (2019). Spatio-temporal geomorphological and ecological dynamics of the Lanphere transgressive dunefield system, Arcata, California. *Global and Planetary Change*, 172: 88-103.

Portz, L., Manzolli, R.P., Hermanns, L., Alcantara Carrio, J.A., Rockett, G.C. & Barboza, E.G. (2021). Degradation of a transgressive coastal dunfield by pines plantation and strategies for recuperation (Lagoa Do Peixe National Park, Southern Brazil). *Estuarine, Coastal and Shelf Science*, 259, 107483.

Provoost, S., Jones, M.L.M. & Edmondson, S.E. (2011). Changes in landscape and vegetation of coastal dunes in northwest Europe: a review. *Journal Coastal Conservation*, 15:207-226.

Pye, K. (1990). Physical and human influences on coastal dune development between the Ribble and Mersey estuaries, northwest England. *In Nordstrom, K. F., Psuty, N. P., & Carter, R. G. W. 5Eds.), Coastal Dunes. Form and Process*, 339-359.

Rickard, C.A., McLachlan,, A. & Kerley, G.I.H. (1994). The effects of vehicular and pedestrian traffic on dune vegetation in South Africa. *Ocaen & Coastal Management*, 23 (3), 225-247.

Ribas, F., Falques, A., Van Den Berg, N. & Caballeria, M. (2013). Modelling shoreline sand waves on the coasts of Namibia and Angola. International. *Journal of Sediment Research*, 28, 1-11.

Robin, N. & Levoy, F. (2007). Stage and rate of formation of a complex spit in a megatidal environment. *Zeitschrift für Geomorphologie*, 51, 337–360.

Robin, N., Levoy, F., Monfort, O. & Anthony, E. (2009). Short-term to decadal-scale onshore bar migration and shoreline changes in the vicinity of a megatidal ebb delta. *Journal of Geophysical Research*. Available at: doi.org/10.1029/2008JF001207

Robin, N., Levoy, F., Anthony, E.J. & Monfort, O. (2020a). Sand spit dynamics in a large tidal-range environment: Insight from multiple LiDAR, UAV and hydrodynamic measurements on multiple spit hook development, breaching, reconstruction, and shoreline changes. *Earth Surf. Process. Landforms*, 45, 2706–2726.

Robin, N., Billy, J., Castelle, B., Hesp, P., Laporte-Fauret, Q., Nicolae-Lerma, A., Marieu, V., Rosebery, D., Bujan, S., Destribats, B. & Michalet, R. (2020b). Beach-dune Recovery from the Extreme 2013-2014 at Truc Vert Beach, Southwest France: New Insights from Ground-Penetrating Radar. *In: Malvárez, G. and Navas, F. (eds.), Proceedings from the International Coastal Symposium (ICS) 2020 (Seville, Spain). Journal of Coastal Research, Special Issue No. 95.* Coconut Creek (Florida). 588-592.

Robin**,** N., Billy, J., Castelle, B., Hesp, P.A., Nicolae-Lerma, A., Laporte-Fauret, Q., Marieu, V., Rosebery, D., Bujan, S., Destribats, B. & Michalet, R. (2021). 150 years of Foredune initiation and evolution driven by human and natural processes. *Geomorphology*, 107516.

Robinet, A., Idier, D., Castelle, B. & Marieu, V. (2018). A reduced-complexity shoreline change model combining longshore and cross-shore processes : the LX-Shore model. *Environ Model Softw*, 109: 1-16.

Rockett, G. C., Barboza, E. G., Fagundes, M. R., Hesp, P. A. & da Camara Rosa, M. L. C. (2021). Evolutionary stage, anthropogenic activities and evolution of the Itapeva dunefield (Torres-RS, Brazil). *Quaternary and Environmental Geosciences*, 12 (2): 01-18.

Seeliger, U. (2003). Response of southern Brazilian coastal foredunes to natural and human-induced disturbance. *Journal of Coastal Research*, SI 35, 51-55.

Short, A. D. (1988). Holocene coastal dune formation in southern Australia: a case study. *Sedimentary geology*, *55*(1-2), 121-142.

Short, A. D. & Hesp, P. A. (1982). Wave, beach and dune interactions in Southeastern Australia. *Marine Geology*, 48 (3-4), 259-284.

Silveira, M. R. D., Dillenburg, S.R. & Barbosa, E. (2022). Morfodinâmica do Sistema Praia-Duna da Barreira Costeira Holocênica do Siriú, Garopaba. *SC. Revista Brasileira de Geomorfologia*, 23(3):1524-1547.

Tastet, J.P. and Pontee, N. (1998). Morpho-chronology of coastal dunes in medoc. A new interpretation of holocene dunes in southwestern France. *Geomorphology*, 25, 93-109.

Thevenot, M.M. & Kraus, N.C. (1995). Longshore sandwaves at Southampton beach, New York: Observations and numerical simulation of their movement. *Marine Geology*, 126, 249-269.

Thompson, L.M.C. & Sclacher, T.A. (2008). Physical damage to coastal dunes and ecological impacts cuased by vehicle tracks associated with beach camping on sand shores: a case study from Fraser Island, Australia. *Journal of Conservation*, 12, 67-82.

Tsoar, H. (2005). Sand dune mobility and stability in relation to climate. *Physica A*, 357: 50-56.

Tsoar, H. & Blumberg, D.G. (2002). Formation of parabolic dunes from barchan and transverse dunes along Israel's Mediterranean coast. *Earth Surf. Process. Landforms*, 27, 1147–1161.

Vitousek, S., Barnard, P.L., Limber, P., Erikson, L. & Cole, B. (2017). A model integrating longshore and cross-shore processes for predicting long-term shoreline response to climate change. *Journal of Geophysical Research: Earth Surface*, 122, 782-806.

Yizhaq, H., Ashkenazy, Y. & Tsoar, H. (2007). Why do active and stabilized dunes coexist under the same climatic conditions? *Physical Review Letters*, 98, 188001.

Zingg, A.W. (1953). Wind tunnel studies of the movement of sedimentary material. Proc. 5th Hydraulic Conf., Bull., vol. 34. Institute of Hydraulics, Iowa City, pp. 111-135.

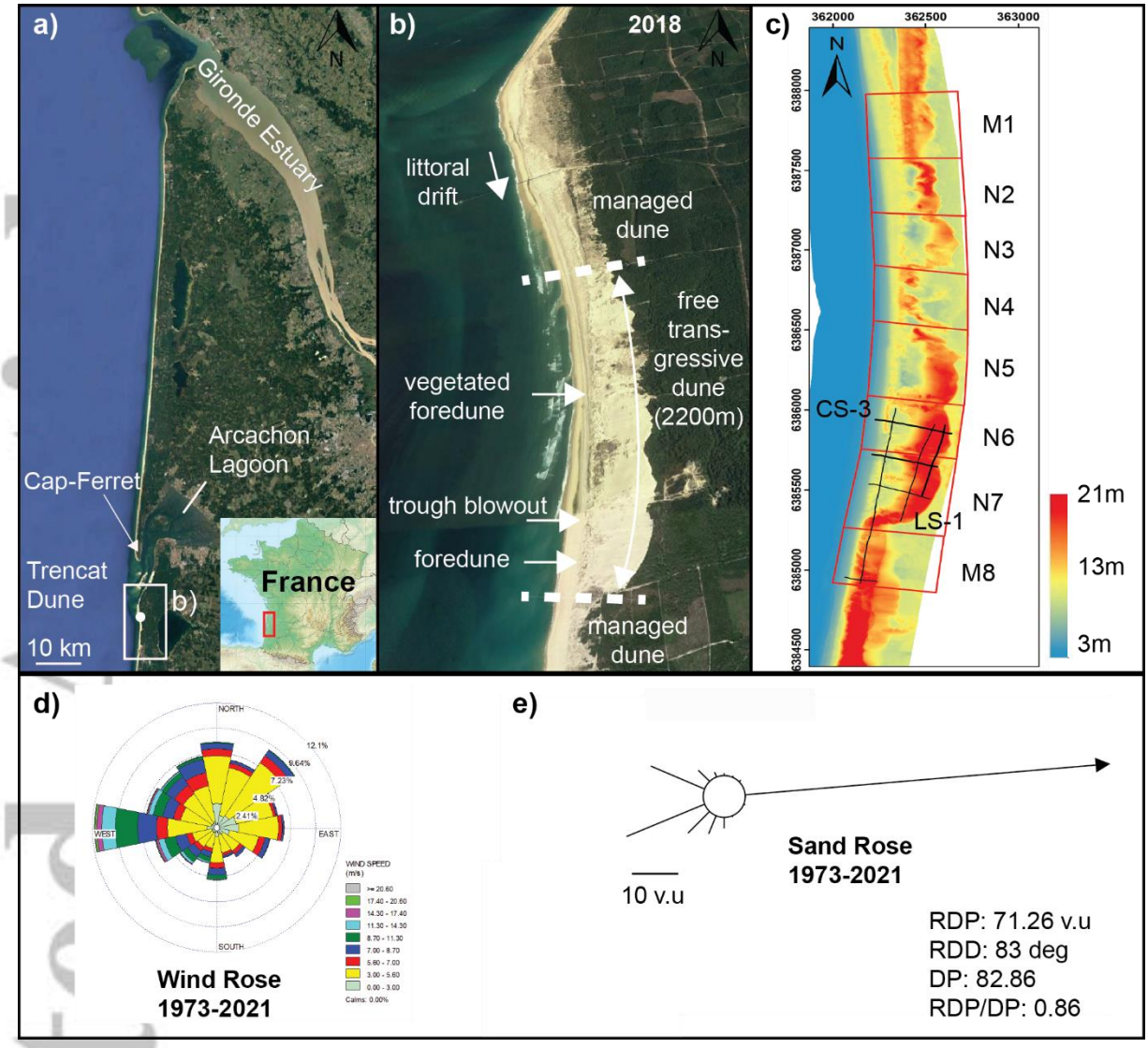

FIGURE 1. (a) Location map. (b) Oblique aerial view (2018) of the Trencat dune (photograph by ONF). (c) Trencat dune topography (LiDAR 2020) GPR (CS and LS) profiles. The field site was divided into six natural areas (N2 to N7) and two managed areas (M1 and M8). (d) Wind rose for the region for the period 1973 – 2021 (Cap Ferret wind station). Note that there is no data available from the meteorological station for the period 1992-1998. (e) Fryberger and Dean sand rose for the region. The individual lines indicate aeolian drift potential (DP) for each direction and the arrow indicates the net resultant aeolian drift potential (RDP) and magnitude (in vector units).

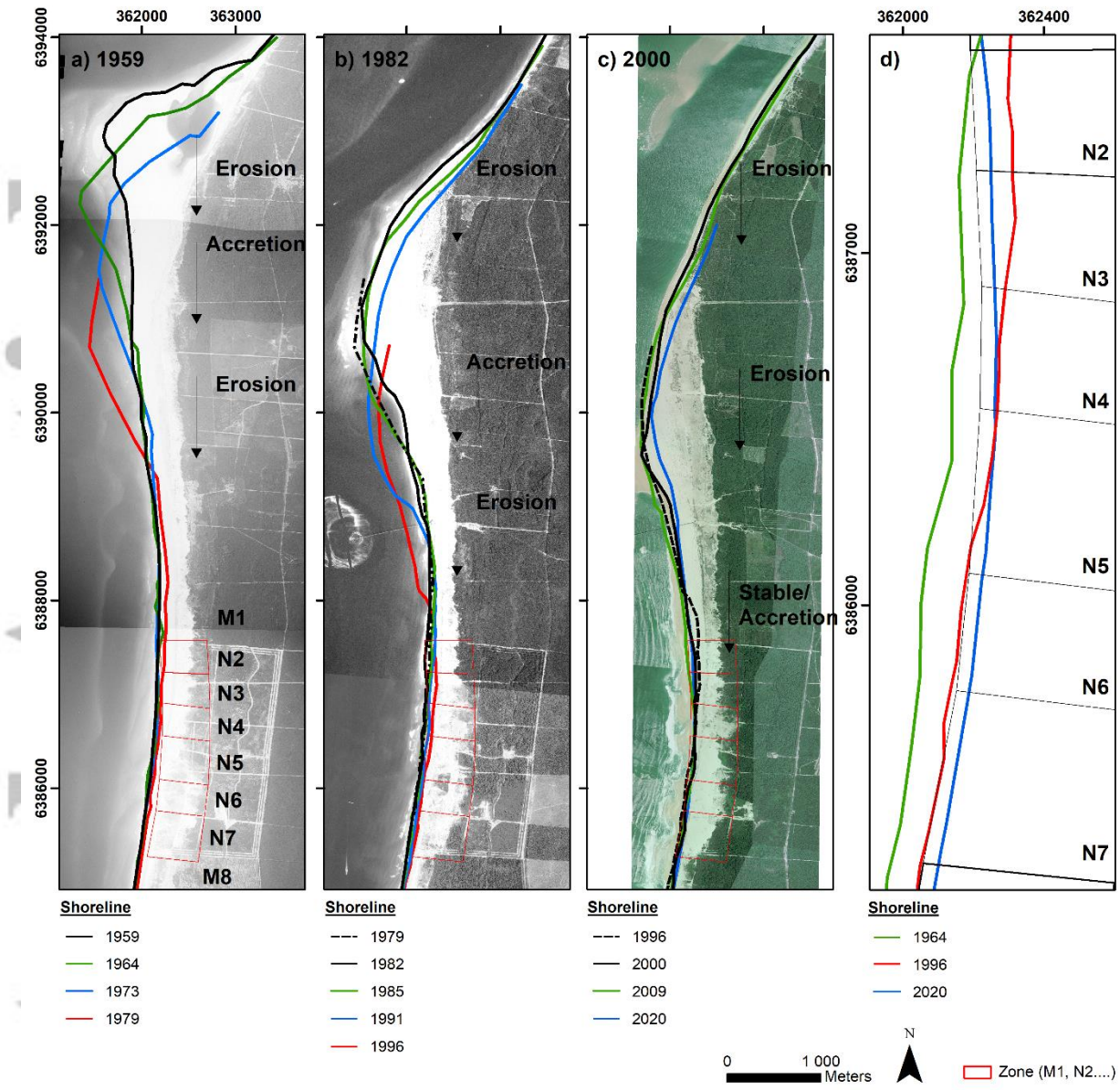

FIGURE 2. Water line position in (a) 1959, (b) 1982 and (c) 2000 illustrating the sand bar welding in 1959 and its southward migration as a sand wave during Stage II and III. Erosion on its downdrift end is observed until 1996 where the littoral drift is less disturbed by its marked geometry. (d) Zoom of the water line position in front the field site. The evolution of sand/woodland (L_{wl}) and dune foot (L_{df}) limit during these periods are indicated in Table 2.

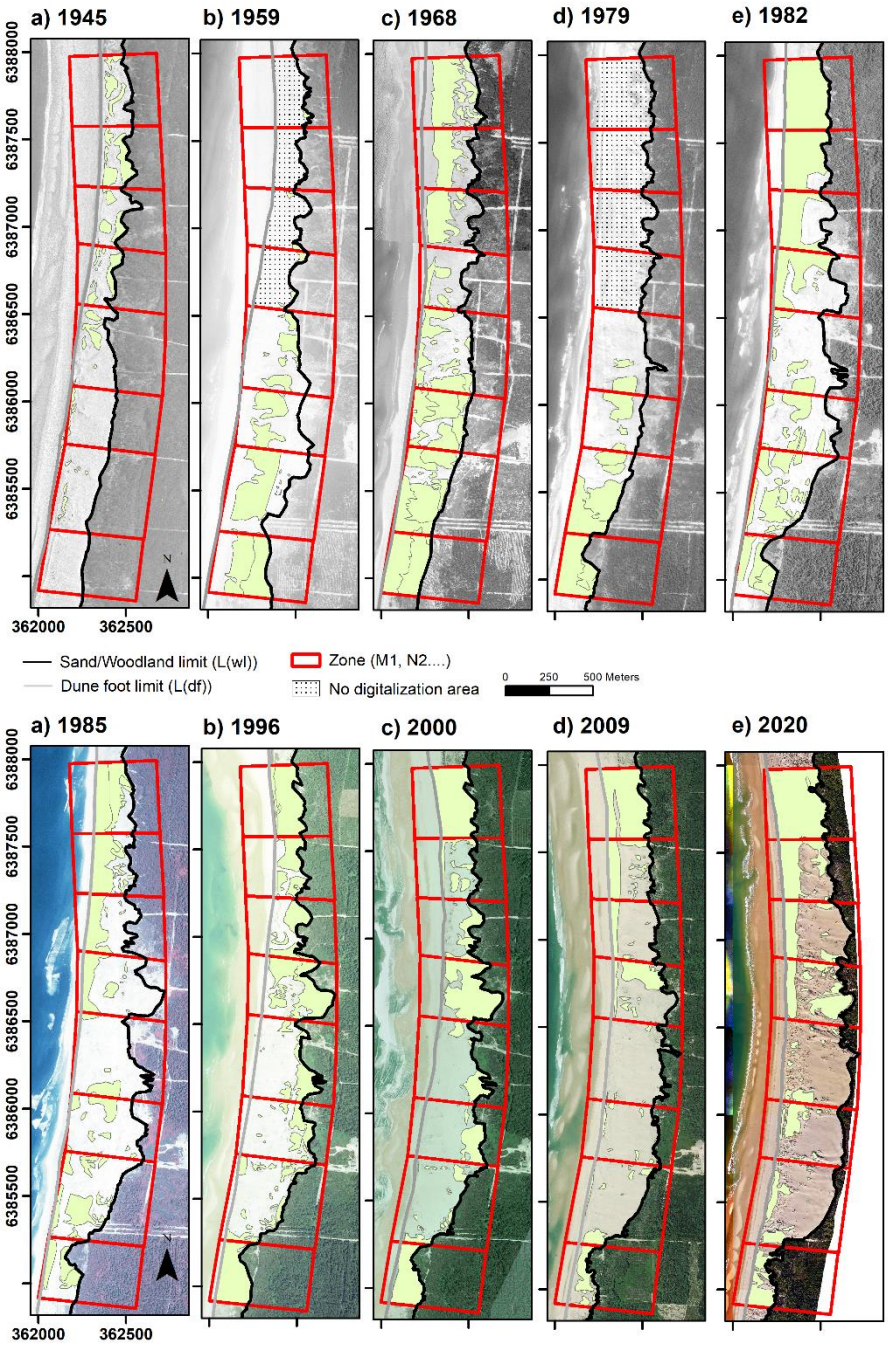

FIGURE 3. Selected aerial photographs and distribution of the cover vegetation. The position of sand/woodland (L_{wl}) and dune foot (L_{df}) limits are indicated.

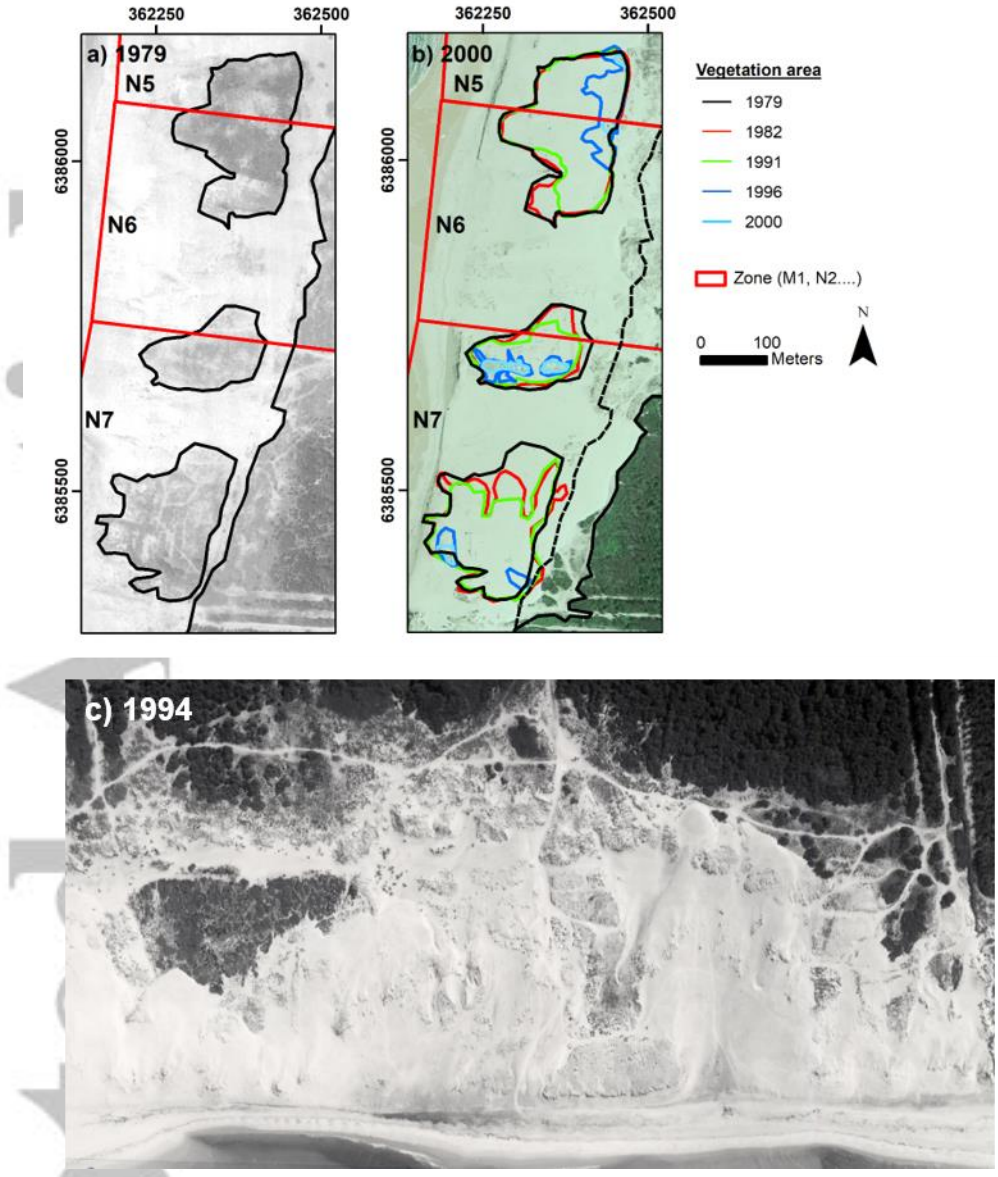

FIGURE 4. Vegetated surfaces on N_5 to N_7 area for (a) 1979 and (b) 2000. (c) Oblique aerial view of the N_5 to N_7 area in 1994 illustrating the destabilization of the system with many blowouts, breaches, large deflation areas and ramps.

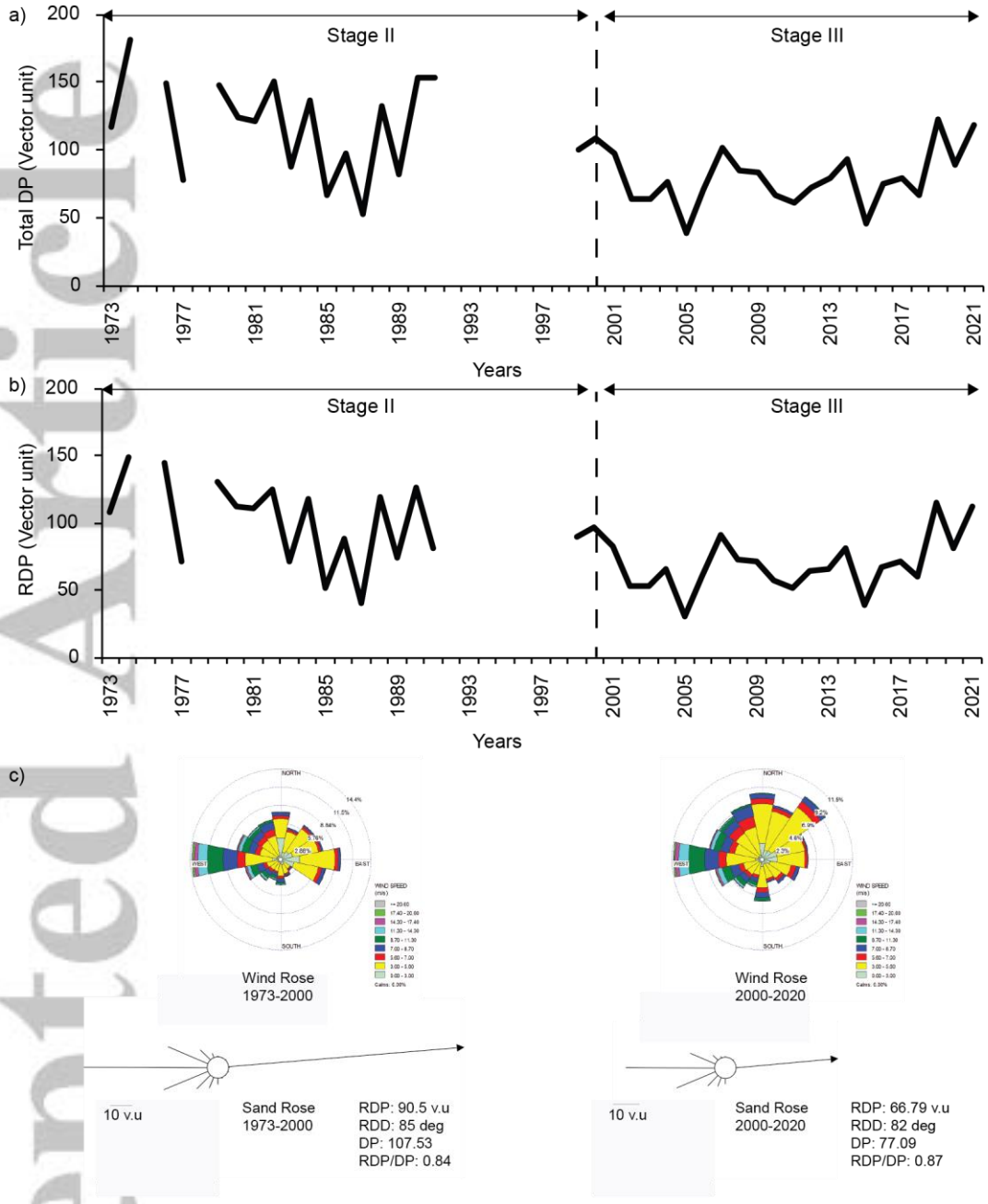

FIGURE 5. (a) Total annual aeolian Drift Potential (DP), (b) Aeolian Resultant Drift Potential (RDP) and (c) Wind rose and Sand rose during the periods 1973-2000 (data of 1992-1998 period is missing) and 2000-2020 for the Trencat dunefield region are indicated.

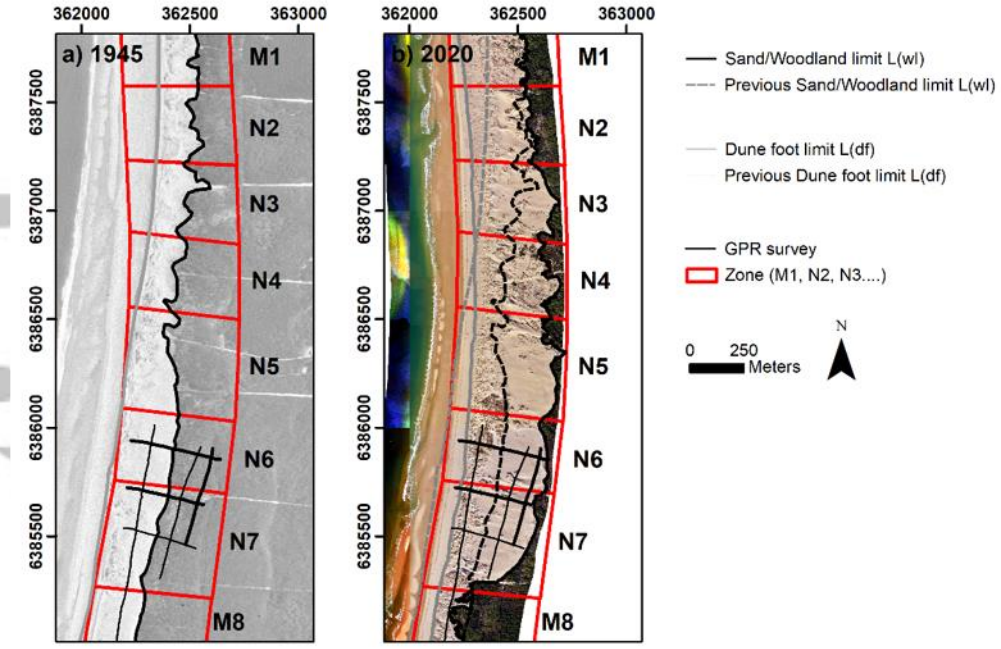

c)	L(wl) evoltion 2020-1945 (m/yr)	L(df) evolution 2020-1945 (m/yr)	Mean Width 1945 (m)	Mean width 2020 (m)	Width evolution 2020-1945 (m)	Width evolution 2020-1945 (%)
M1	0,1	1,9	150	286	136	90
N2	-0,4	1,0	169	282	113	67
N3	-1,8	0,4	172	344	172	100
N4	-2,7	-0,3	161	342	181	112
N5	-3,1	-1,0	217	374	157	73
N6	-2,7	-1,4	276	370	94	34
N7	-2,7	-1,4	260	356	96	37
M8	0,4	-1,2	263	144	-119	-45

FIGURE 6. Residual evolution of the sand/woodland (L_{wl}) and dune foot (L_{df}) limits between (a) 1945 and (b) 2020. The table (c) shows the L_{wl} and L_{df} rates and width evolution for each area.

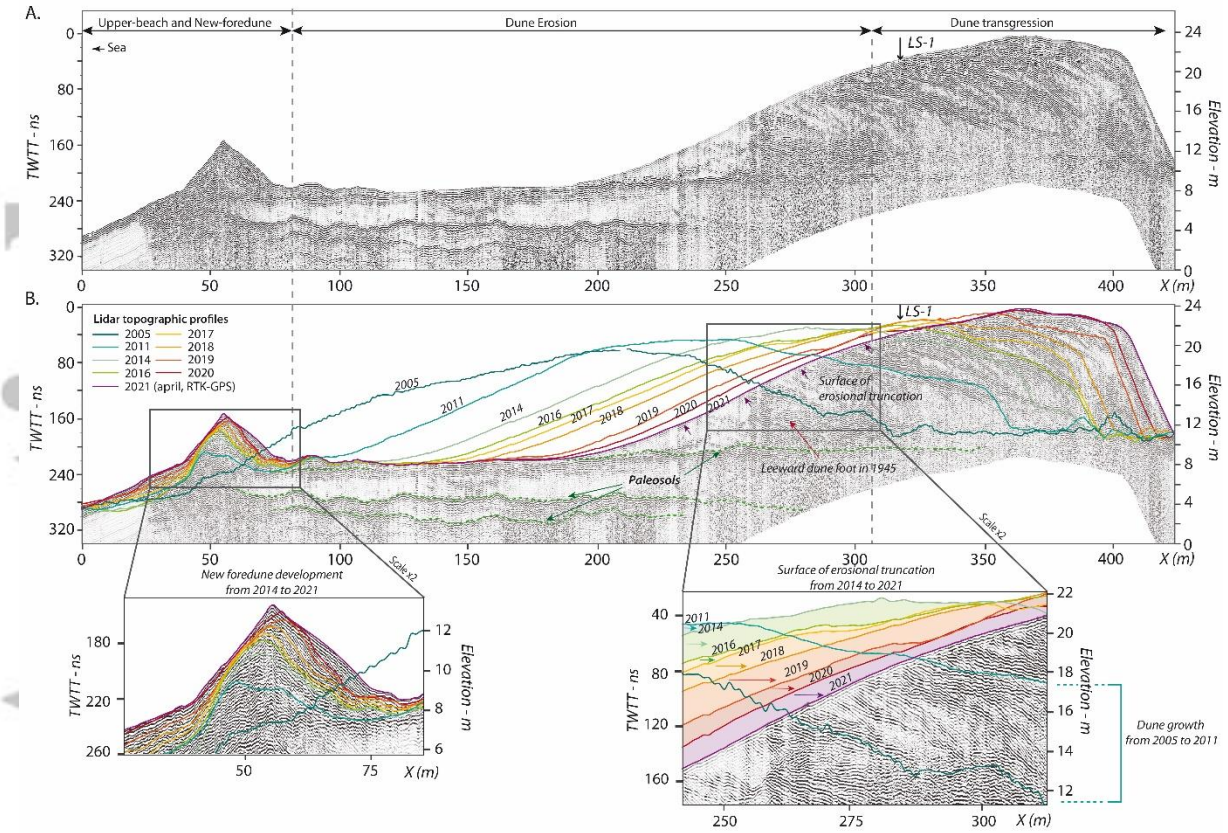

FIGURE 7. (a) Processed versions of the profile CS-3 acquired with 500 MHz frequency antennae. GPR data are given in nanosecond (ns) two-way travel time (TWTT) and elevations are with reference to mean sea-level (amsl). (b) Topographic survey drawn on (a). Localization of LS-1 is indicated and also the leeward dune foot position in 1945.

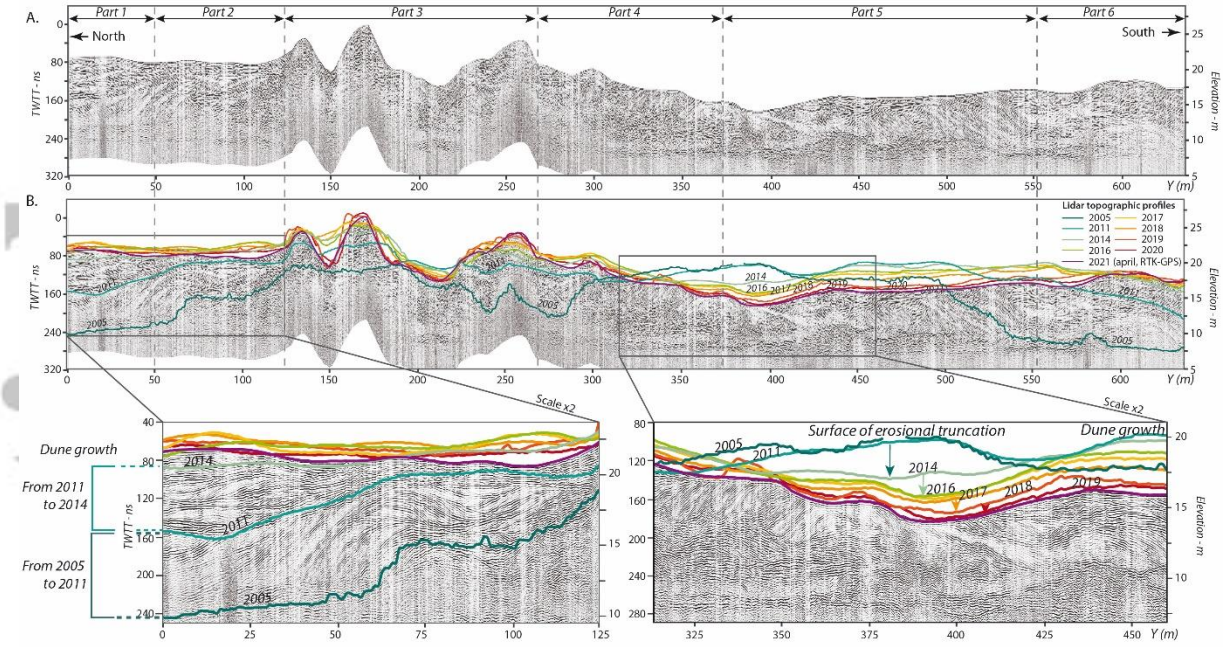

FIGURE 8. (a) Processed versions of the profile LS-1 acquired with 500 MHz frequency antennae. GPR data are given in nanosecond (ns) two-way travel time (TWTT) and elevations are with reference to mean sea-level (amsl). (b) Topographic survey drawn on (a). Localization of LS-1 is indicated.

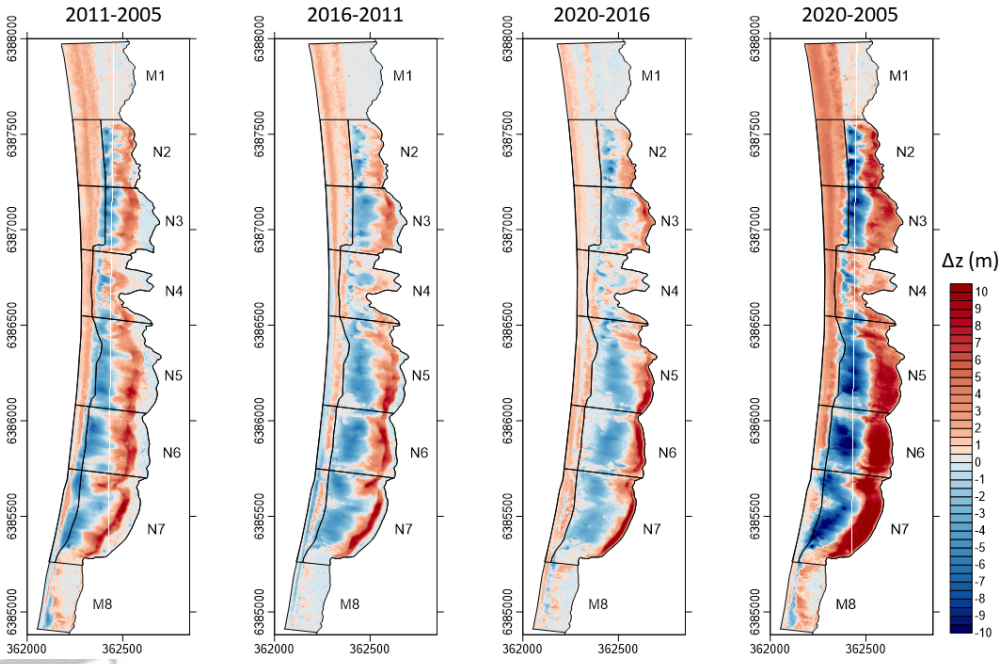

FIGURE 9. DTM difference plot of the Trencat dune during different periods of Stage III. Black lines correspond to the limits of the foredune, transgressive dune and landward dune, and of each area.

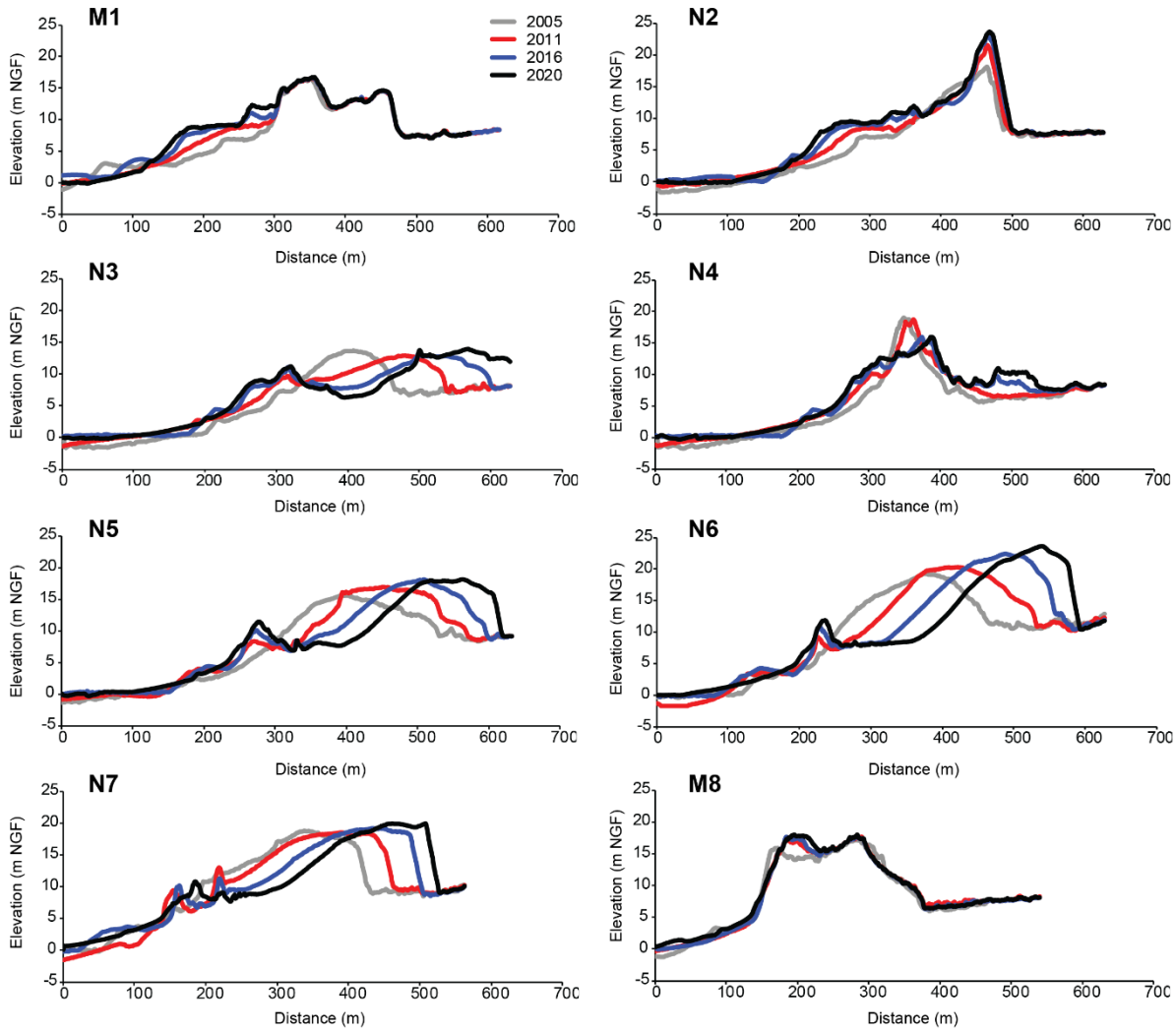

FIGURE 10. Cross-shore profile evolution (M_1 to M_8) during Stage III.

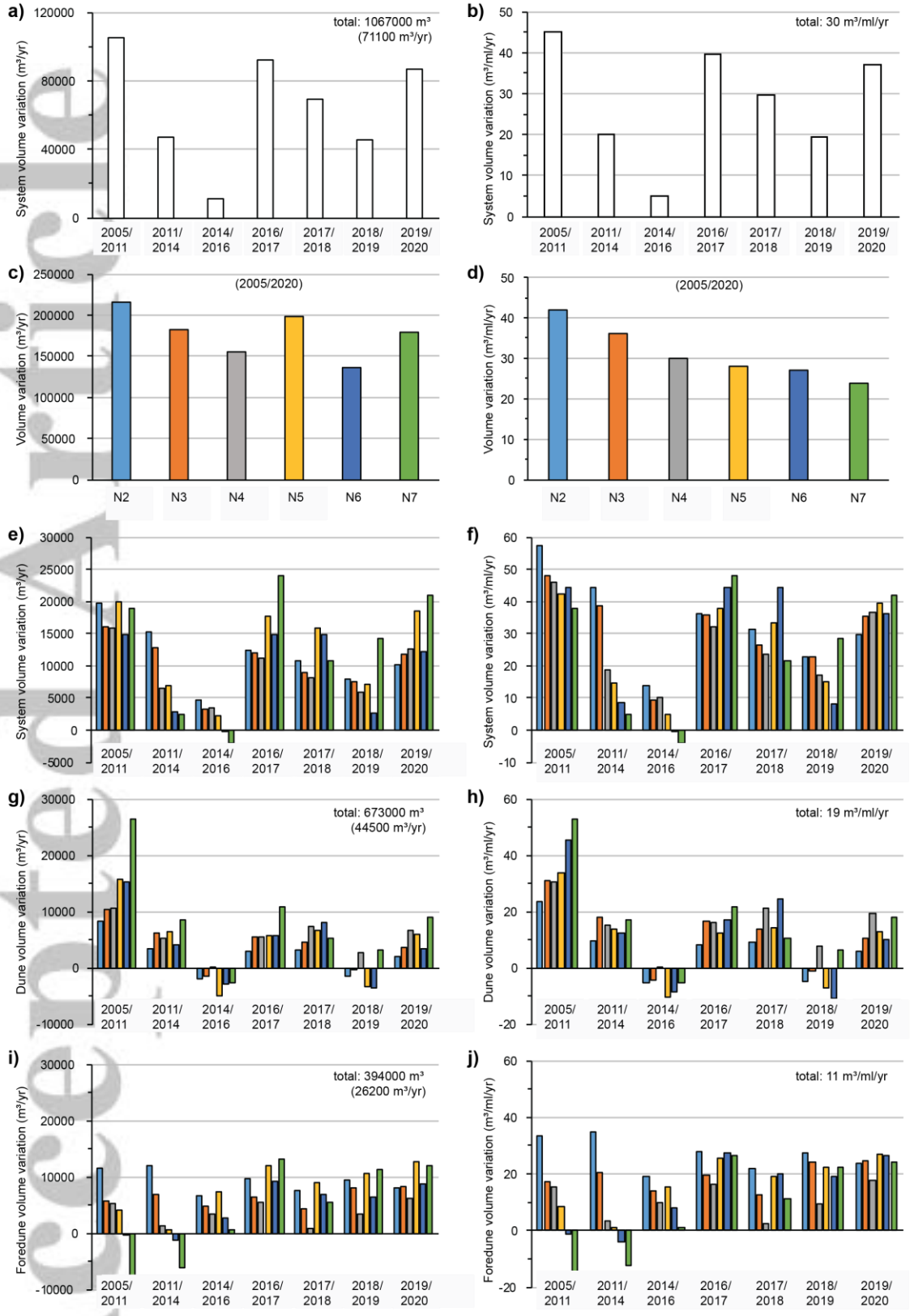

FIGURE 11. Sand volume analysis. (a) Volume change between each survey; (c) overall changes between 2005 and 2020 with areas discriminated; (e) changes between each survey and by area with (g) and (i) the same but for the transgressive dune and the foredune, respectively. The corresponding right-hand panels show the same changes but per beach width (m^3/ml/yr).

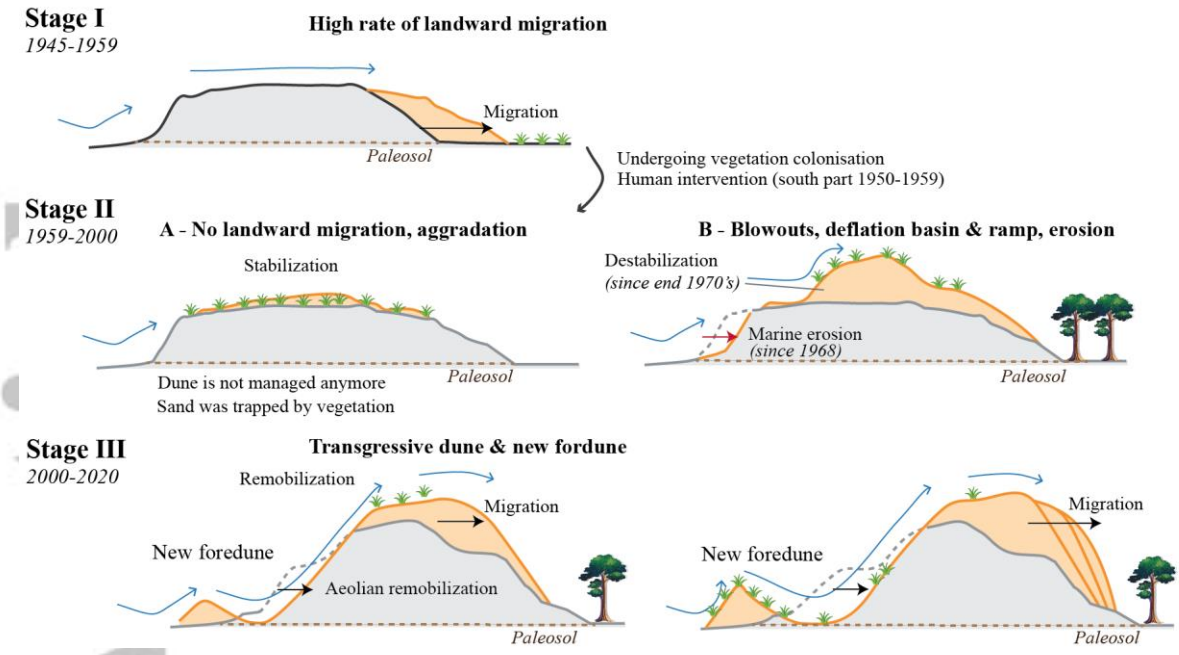

FIGURE 12. Conceptual model of the evolution stages of the Trencat dune between 1949 and 2020 applied on the southern part. Stage I where the dune migrates landwards at a similar height; Stage II comprising stabilization (1959-1968) then shoreline erosion and destabilization state; Stage III comprising the remobilization with foredune formation, significant deflation and cannibalization of the dune system with landwards migration and development of a high slipface/precipitation ridge. Scales are not respected.

Table.1: Details of uncertainties of photographs and LiDAR.

Date	**Source**	**Type**	**Mean Ground resolution (m)**	**RMS error (m)**	**Onscreen delineation (m)**	**Total uncertainty (m)**
1945 to 1982	IGN	B&W/Raster	0.7	< 3	2	5
1985 to 1998	IGN	Color/Raster	0.59	< 3	2	5
2000 to 2020	IGN/OCA	Color/Ortho	0.26	0.2	2	2.5
Date	**Source**	**Type**	**Altimetric error Z (m)**			
2005, 2011, 2014	OCA	LiDAR	0.235, 0.196, 0.144			
2016, 2017, 2018	OCA	LiDAR	0.106, 0.102, 0.096			
2019, 2020	OCA	LiDAR	0.098, 0.078			

Table 2. The evolution of (A) sand/woodland (L_{wl}) and (B) dune foot (L_{df}) limits during the survey period (1945-2020). Rates are negative (positive) landwards (seawards) and NS = not significant evolution. Zone locations are shown in Figure 1. Vg+ (Vg-) is the gain (destruction) of vegetation without dune migration. Position of L_{df} in 1979 is not indicated due to the brightness of the photography.

A) L_{wl} (m/yr)	**Stage I**		**Stage II**									***Stage III***			
Period	***1945-1950***	***1950-1959***	***1959-1964***	***1964-1968***	***1968-1973***	***1973-1979***	***1979-1982***	***1982-1985***	***1985-1991***	***1991-1996***	***1996-2000***	***2000-2005***	***2005-2009***	***2009-2016***	***2016-2020***
M1	-3.8	*NS*	*NS*	*NS*	*NS*	*NS*	*NS*	*NS*	*NS*	*NS*	*NS*	*NS*	*NS*	*NS*	*NS*
N2	-2.2	*NS*	*NS*	*NS*	*NS*	*NS*	*NS*	*NS*	*NS*	*NS*	*NS*	-1.0	*-3.0*	*NS*	*NS*
N3	-10.2	**Vg+**	*NS*	*NS*	*NS*	*NS*	*NS*	*NS*	*NS*	*NS*	*NS*	*NS*	*-6.7*	*-6.3*	*-4.1*
N4	-12.4	**Vg+**	*NS*	*NS*	-4.9	*NS*	-23.7	-12.1	*NS*	*NS*	**Vg-**	-1.2	*-6.9*	*NS*	*NS*
N5	-23.1	*NS*	**Vg+**	*NS*	*NS*	*NS*	**Vg-**	*NS*	*NS*	*NS*	*NS*	-2.7	*-10.6*	*-2.6*	*-6.3*
N6	-21.6	-1.5	**Vg+**	*NS*	*NS*	*NS*	**Vg-**	*NS*	*NS*	*NS*	*NS*	*NS*	*-2.5*	*-3.1*	*-5.7*
N7	-15.9	-5.8	**Vg+**	*NS*	*NS*	*NS*	**Vg-**	*NS*	*NS*	*NS*	*NS*	-2.2	*-5.1*	*-4.7*	*-6.1*
M8	-10.8	-4.1	*NS*	**Vg+**	*NS*	**Vg+**	**Vg-**	*NS*	*NS*	*NS*	*NS*	*NS*	*NS*	*-0.8*	*NS*
Uncertainty (m/yr)	2.07	1.10	1.96	2.90	1.72	1.70	3.45	3.42	1.64	2.06	2.58	1.00	*1.25*	*0.67*	*1.26*

B) L_{df} (m/yr)	**Stage I**		**Stage II**								**Stage III**			
Period	***1945-1950***	***1950-1959***	***1959-1964***	***1964-1968***	***1968-1973***	***1973-1982***	***1982-1985***	***1985-1991***	***1991-1996***	***1996-2000***	***2000-2005***	***2005-2009***	***2009-2016***	***2016-2020***
M1	*NS*	-1.4	19.8	7.2	-5.8	-2.1	-9.1	-2.9	-1.9	34.8	-12.3	*NS*	7.2	*NS*
N2	-2.9	-1.3	22.8	7.9	-4.6	-2.8	-7.1	*NS*	-11.1	24.4	-9.0	4.2	4.1	*NS*
N3	*NS*	-1.1	18.3	*NS*	*NS*	-2.7	-2.5	-2.7	-10.7	*NS*	1.6	2.9	3.3	*NS*
N4	*NS*	*NS*	10.7	-6.9	2.6	*NS*	-4	-3.2	-8.9	-8.7	2.6	*NS*	2.1	2.8
N5	*NS*	*NS*	2.4	*NS*	1.9	*NS*	-3.4	-2.9	-6.6	-8.9	-1.3	1.8	-0.7	4.0
N6	*NS*	*NS*	*NS*	*NS*	2.2	-1.2	-3.2	-2.7	-4.8	-6.2	-7.5	*NS*	-1.1	1.8
N7	-2.5	*NS*	*NS*	-5.4	2.4	*NS*	-2.5	*NS*	-5.5	-7.3	-3.5	*NS*	-1.9	*NS*
M8	*NS*	*NS*	*NS*	-5.6	2.2	*NS*	-1.9	-2.0	-3.0	-3.3	-7.3	2.2	*NS*	*NS*
Uncertainty (m/yr)	2.1	1.1	2.0	2.9	1.7	1.1	3.4	1.6	2.1	2.6	1.0	1.2	0.7	1.3

Table 3 : Residual sand volume change between 2005 and 2020 (Stage III) for each part and area of the dune field.

		System volume		Foredune volume		Dune volume		Back dune volume	
		m^3	m^3/m	m^3	m^3/m	m^3	m^3/m	m^3	m^3/m
2005-2020	***N2***	216 400	630	156 500	455	59 850	170	250	1
	N3	182 300	540	93 100	280	89 200	270	-5 250	-16
	N4	155 500	450	55 700	160	99 750	290	2 300	7
	N5	198 300	420	82 900	180	115 400	250	-7 500	-16
	N6	136 300	410	28 700	85	107 650	320	-7 600	-23
	N7	178 700	360	-23 000	-45	201 650	400	975	2
	Total	1 067 500	-	393 900	-	673 500	-	-16 825	-
	Mean	-	468	-	185	-	283	-	-8

Studies quantifying the dynamics of transgressive dunefields at meso-scale (10^1-10^{10} years) timeframes and/or sedimentary assessment of the system in 3D are scarce. Results of aerial photographs, GPR and recent LiDAR surveys show two periods of landward migration (1945-1959 and 2000-2020), separated by ~40 years of stablility. The dune has grown in volume (600,000 m^3 between 2005-2020) and the sand supply from the beach to the dunefield is therefore still significant despite the formation of the post-2005 foredune (400,000 m^3).